Computers and Structures 138 (2014) 142–161

Contents lists available at ScienceDirect

Computers and Structures

journal homepage: www.elsevier.com/locate/compstruc

A three-dimensional multilayered pipe beam element: Nonlinear analysis

L.L. Aguiar [a], C.A. Almeida [b], G.H. Paulino [c,*]

[a] Petrobras, CENPES – Research and Development Center, Rio de Janeiro, Brazil
[b] Department of Mechanical Engineering, Pontifical Catholic University of Rio de Janeiro, Rio de Janeiro, Brazil
[c] Department of Civil and Environmental Engineering, University of Illinois, Urbana, IL 61801, USA

ARTICLE INFO

Article history:
Received 26 March 2013
Accepted 26 September 2013
Available online 21 April 2014

Keywords:
Multi-layered pipe beams
Interlayer slip
Finite element
Nonlinear analysis

ABSTRACT

This paper addresses the behavior of three-dimensional multilayered pipe beams with interlayer slip condition, under general 3-D large displacements, in global riser and pipeline analysis applications. A new finite element model, considering the Timoshenko beam for each element layer, has been formulated and implemented. It comprises axial, bending and torsional degrees-of-freedom, all varying along the length of the element according to discretization using Hermitian functions: constant axial and torsional loadings, and linear bending moments. Transverse shear strains due to bending are included in the formulation by including two generalized constant degrees-of-freedom. Nonlinear contact conditions, together with various friction conditions between the element layers, are also considered. These are accounted in the model through a proper representation of the constitutive relation for the shear stress behavior in the binding material. The element formulation and its numerical capabilities are evaluated by some numerical testing results, which are compared to other numerical or analytical solutions available in the literature. The tests results show that the new element provides a simple yet robust and reliable tool for general multilayered piping analyses.

1. Introduction

Multilayered pipelines have been widely used in the petroleum industry to transport almost all types of fluids in the oil production system. Flexible lines are the most common example of this type of structure, which consists of a tubular arrangement of concentric metallic and polymeric material layers. Although widely in use, appropriate representation of flexible lines in numerical simulation still represents a great numerical challenge, mainly due to their nonlinear dynamic behavior in global riser analysis and to nonlinearities caused by its multilayered cross section.

An alternative to flexible lines is the use of steel rigid lines, which also have static (pipelines) and dynamic (risers) applications. As well as flexible lines, the rigid pipelines often have multilayered cross section, due to internal corrosion resistant alloys (CRA) and external thermal insulation coatings. In both, mechanical design and global riser analyses, the presence of these additional layers are neglected, mainly due to difficulties of current available numerical models to adequately represent the behavior of multilayered pipes.

In the literature, several analytical and numerical solutions have been proposed since Newmark et al. [1] first proposed a two-layered Euler–Bernoulli beam model considering linear behavior. More recently, Schnabl et al. [2], Foraboschi [3] and Ecsedi and Baksa [4], proposed analytical solutions for two-layered laminated beams considering interlayer slip condition, but restricted to small displacements and linear constitutive models for each layer material. Some of these papers also included transverse shear deformation in their formulation. Attempts for more general analytical solutions have been proposed by Girhammar and Gopu [5] and Girhammar and Pan [6] who presented exact solutions, for first and second order analysis procedures, allowing estimation of the magnitude of beam deformation and internal actions between layers. Chen et al. [7] presented a solution where the combined action of arbitrary transverse and constant axial loadings, under static conditions, is considered in a non-uniform slip stiffness model. In the same line of investigation, numerical methods were also proposed by many authors, mainly based on the finite element method (FEM) approach. A strain-based FEM, based on the Timoshenko beam theory for each element layer, applicable to linear static analysis of two-layer planar composite beams, with interlayer slip, was proposed by Schnabl et al. [8]. Using a similar approach, Čas et al. [9,10] presented a finite element formulation that considers non-linear time-dependent constitutive models for

* Corresponding author. Tel.: +1 2173333817; fax: +1 2172658041.
E-mail addresses: ludiaguiar@gmail.com (L.L. Aguiar), calmeida@puc-rio.br (C.A. Almeida), paulino@uiuc.edu (G.H. Paulino).

http://dx.doi.org/10.1016/j.compstruc.2013.09.005
0045-7949/

the element layers and a non-linear relationship between the slip and the shear stress at the interface. In this formulation, the geometrically non-linear Reissner's beam theory was used. Krawczyk and Frey [11,12], proposed a 2D beam element for geometric non-linear analysis of multilayered beams considering interlayer slip. The element formulation is based on the co-rotational approach with Timoshenko's beam theory assumptions. The element is assumed to undergo large displacements and rotations, but with small deformations and moderate slip between layers. A 2D model comparing the FEM solutions with extended Euler–Bernoulli's formulation and Timoshenko's beam model of slab beams for various loadings was presented by Zona and Ranzi [13]. It is shown that displacement and stress results in composite members are controlled by the interaction between bending and shear (short or long beams), in each case study. The behavior of general multi-stacked composite beams with interlayer slip was considered by Sousa Jr. and Silva [14] for the rectangular section where curvature locking difficulties were identified. Their model represents the composite beam as an association of beams and interface elements, providing an efficient solution for the multilayered beam problem.

Several studies on multilayer beams are now available in the literature. However most of them have their application limited to laminated beams under in plane loading only. To the best of author's knowledge, an appropriate representation of multilayered pipes in three-dimensional nonlinear analysis has not yet been addressed in the literature.

In this work, a multilayered pipe beam formulation, which accounts for axial and bending degrees-of-freedom at each layer is proposed. It includes classical modes of deformation and nonlinear interlayer slip (with shear deformation assumed constant through the interlayer material thickness). In this model, damage at the interface is accounted by considering a yielding-type function for the interface material constitutive model, in a nonlinear fashion of analysis. The FEM formulation considers the nonlinear behavior of multilayered pipes under general 3-D large displacements. An updated Lagrangian formulation is employed including large displacements and rotations. The conventional two-node Hermitian displacement functions [15] are employed to represent the element in convected (co-rotated) coordinates. The element combines Euler–Bernoulli beam solutions, with constant transverse shear strains along the length, by adding two generalized degrees-of-freedom to the conventional axial, bending and torsional ones. The additional shear degrees-of-freedom are statically condensed throughout the solution procedure. Interface binding conditions, which have been considered in previous 2-D models, are also included in the 3-D element model formulation, and are dealt within a unique and novel fashion, allowing the element to represent the behavior of multilayered pipes in non-linear static analysis. A few representative solutions are presented and compared to other independently obtained numerical results.

The contributions of this work are: novel nonlinear formulation for tubular pipes that are used as risers in the offshore industry; treatment of interfaces in multilayered pipes. While there is a plenty of literature in laminated and multilayered plates, such is not the case for multilayered pipes; methodology to couple the interfaces of multilayered pipe systems. For instance, a new interlayer contact model is embedded in a plasticity framework.

2. Multilayered pipe beam element

The multilayered pipe beam FEM presented in this work is based on the co-rotational formulation, which have been the subject of various publications [15–17]. It refers to a straight spatial reference configuration, defined by the updated coordinates of the element two nodal points. In the multilayered element formulation, it is assumed that the element is subjected to large displacements and rotations, but restricted to small strains and small slip condition between layers. Timoshenko hypothesis is assumed for all element layers, i.e., initially plane layer cross sections remain plane and non-deformed in and out of its plane after element deformation, but not necessarily perpendicular to the beam longitudinal axis. Under torsion, cross sections remain plane without warping. All element layers share the same transverse displacements at element nodes i.e., no separation between layers is allowed. In the element formulation, all variables are referred to a co-rotational configuration obtained from geometric transformations, including rigid body translations and rotations, from an initial non-deformed configuration. These variables can be identified from three distinct configurations: initial configuration (C_{ini}) which is represented by the element in its non-deformed configuration, at spatial position $t = 0$, reference configuration (C_{ref}) that is represented by the configuration in which the element has been subjected from its initial position to rigid body motions only, and deformed configuration (C_{def}) that is represented by the element in its current configuration at time t, after moving with rigid body motions and deformations due to applied external loads.

Reference systems attached to the beam element at each configuration are shown in Fig. 1 and are described as follows

- The global system $(\overline{X}\,\overline{Y}\,\overline{Z})$ is a spatial coordinate system whereby the structure is referred to. This system remains fixed during the entire beam analysis;
- The initial local element system $(X'Y'Z')$ is a coordinate system associated to the element at its initial non-deformed configuration (C_{ini}). At this configuration, the element is assumed straight with the X'-axis coinciding with the element longitudinal direction and the other two Y' and Z' axes along the cross section principal directions of inertia;
- The local element system $(X\,Y\,Z)$ is associated to the reference configuration (C_{ref}), which is the initial local element system with rigid body motion. The X-axis lies on the straight line defined by the two element nodes at the updated position. The formulation of the co-rotational element is developed based on this reference system;
- The element layer nodal systems $(x_i^k\ y_i^k\ z_i^k)$ are the coordinate systems associated to each node-i, for each layer-k, in the co-rotational formulation. The nodal systems of each layer are fixed to the element nodes, following its movements (translation and rotation).

2.1. Basic formulation for large rotations

When dealing with a reference vector in 3-D transformations, an orthogonal spatial transformation matrix $\mathbf{R}(\theta)$ should be considered

$$\mathbf{v}_1 = \mathbf{R}(\theta)\mathbf{v}_0 \tag{1}$$

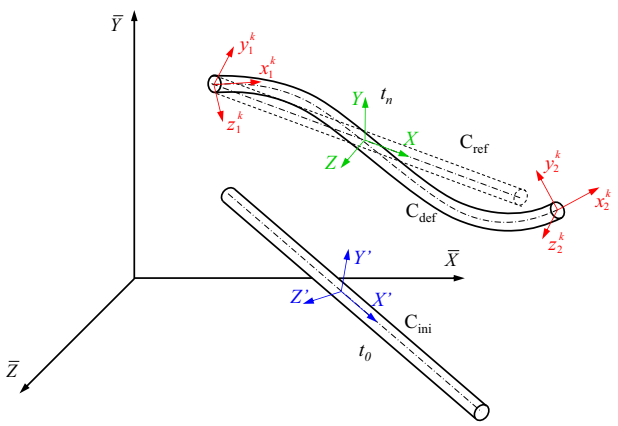

Fig. 1. Beam element reference configurations.

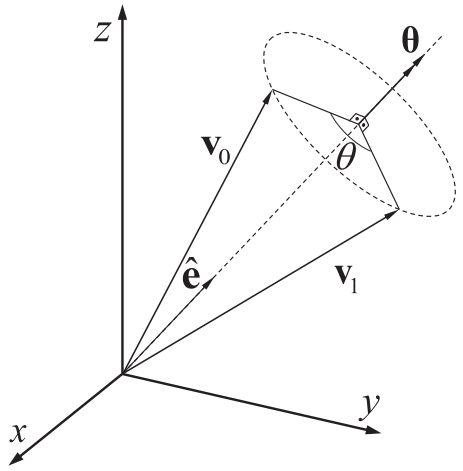

Fig. 2. Spatial transformation between two vectors.

which is represented in terms of only three independent parameters as shown by Pacoste and Eriksson [18]. This approach results from the use of a pseudo-vector of rotation, defined as $\boldsymbol{\theta} = \theta\hat{\mathbf{e}}$, which represents a unique rotation with an angle θ about a fixed axis defined by the unit vector $\hat{\mathbf{e}}$. (see Fig. 2).

In this case, considering the magnitude of the rotation angle $\theta = \sqrt{\theta_x^2 + \theta_y^2 + \theta_z^2}$, the orthogonal rotation matrix (Rodrigues) can be expressed by [17]

$$\mathbf{R} = \mathbf{I} + \frac{\sin\theta}{\theta}\mathbf{S}(\boldsymbol{\theta}) + \frac{1-\cos\theta}{\theta^2}\mathbf{S}(\boldsymbol{\theta})\mathbf{S}(\boldsymbol{\theta}) \tag{2}$$

where $\mathbf{I}$ is the 3×3 identity matrix and $\mathbf{S}(\boldsymbol{\theta})$ is a skew-symmetric matrix obtained from the rotation pseudo-vector components θ_x, θ_y and θ_z, as follows:

$$\mathbf{S}(\boldsymbol{\theta}) = \begin{bmatrix} 0 & -\theta_z & \theta_y \\ \theta_z & 0 & -\theta_x \\ -\theta_y & \theta_x & 0 \end{bmatrix}, \quad \boldsymbol{\theta} = \begin{bmatrix} \theta_x \\ \theta_y \\ \theta_z \end{bmatrix} = \theta\hat{\mathbf{e}} \tag{3}$$

In the co-rotational formulation used in this work, matrix $\mathbf{R}$ as defined in Eq. (2) is used to update the element reference configuration as well as the nodal reference systems.

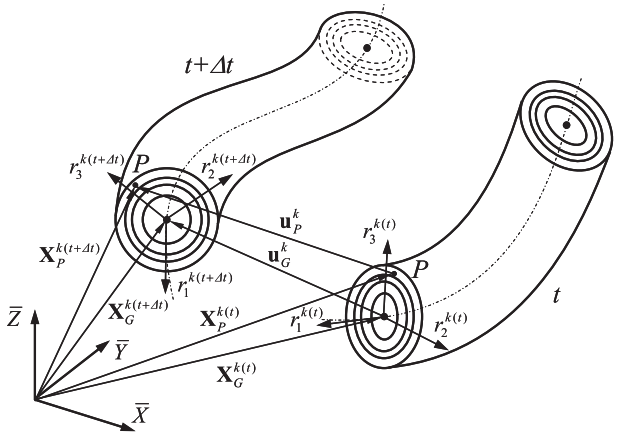

Fig. 3. Multilayer element in two successive configurations.

2.2. Kinematics of deformation

Incremental and iterative analysis is considered in the formulation with all element reference systems (see Fig. 1) being updated after each iteration, i.e., the co-rotational approach is updated at each iteration. In this way, two neighboring configurations of a segment of a pipe beam with multiple layers, in two successive configurations, at instants t and $t + \Delta t$, are as shown in Fig. 3,

where Δt is the time increment, $\mathbf{X}_P^{k(t)}$ and $\mathbf{X}_P^{k(t+\Delta t)}$ are the position vectors of a point P in layer-k cross section, at instants t and $t + \Delta t$, respectively; $\mathbf{X}_G^{k(t)}$ and $\mathbf{X}_G^{k(t+\Delta t)}$ are layer-k geometric center position vectors at instants t and $t + \Delta t$, respectively; point P position in both configurations is expressed in terms of the coordinates (x, y, z) in the local reference system r^k and the geometric center position vector $(\mathbf{X}_G^k)$, i.e.:

$$\begin{aligned} \mathbf{X}_P^{k(t)} &= \mathbf{X}_G^{k(t)} + y\hat{\mathbf{r}}_2^{k(t)} + z\hat{\mathbf{r}}_3^{k(t)} \\ \mathbf{X}_P^{k(t+\Delta t)} &= \mathbf{X}_G^{k(t+\Delta t)} + y\hat{\mathbf{r}}_2^{k(t+\Delta t)} + z\hat{\mathbf{r}}_3^{k(t+\Delta t)} \end{aligned} \tag{4}$$

The incremental displacement vector at point P is then obtained:

$$\begin{aligned} \mathbf{u}_P^k &= \begin{bmatrix} u_P^k & v_P^k & w_P^k \end{bmatrix}^T \\ &= \mathbf{X}_P^{k(t+\Delta t)} - \mathbf{X}_P^{k(t)} \\ &= \mathbf{u}_G^k + y(\hat{\mathbf{r}}_2^{k(t+\Delta t)} - \hat{\mathbf{r}}_2^{k(t)}) + z(\hat{\mathbf{r}}_3^{k(t+\Delta t)} - \hat{\mathbf{r}}_3^{k(t)}) \end{aligned} \tag{5}$$

where $\mathbf{u}_G^k$ is the k-th layer geometric center incremental displacement vector:

$$\mathbf{u}_G^k = \mathbf{X}_G^{k(t+\Delta t)} - \mathbf{X}_G^{k(t)} = \begin{bmatrix} u^k & v & w \end{bmatrix}^T \tag{6}$$

Transformations between the local reference system vectors r_i^k $(i = 1, \ldots, 3)$, shown in Fig. 3, at time t and at time $t + \Delta t$ are obtained from incremental cross section rotations $(\theta_x, \theta_y, \theta_z)$. This transformation is obtained by using a suitable rotation matrix $\mathbf{R}(\theta_x, \theta_y, \theta_z)$,

$$\hat{\mathbf{r}}_i^{k(t+\Delta t)} = \mathbf{R}\hat{\mathbf{r}}_i^{k(t)} \quad (i = 2, 3) \tag{7}$$

Substituting Eq. (7) into Eq. (5), one obtains point P incremental displacements as

$$\mathbf{u}_P^k = \mathbf{u}_G^k + y(\mathbf{R} - \mathbf{I})\hat{\mathbf{r}}_2^{k(t)} + z(\mathbf{R} - \mathbf{I})\hat{\mathbf{r}}_3^{k(t)} \tag{8}$$

An approximation for the rotation matrix presented in Eq. (2) is obtained by considering terms up to second order from the series expansion of the trigonometric terms. Thus, the Rodrigues formula results in the following rotation matrix:

$$\mathbf{R} = \begin{bmatrix} 1 - \frac{\theta_y^2 + \theta_z^2}{2} & -\theta_z + \frac{\theta_x\theta_y}{2} & \theta_y + \frac{\theta_x\theta_z}{2} \\ \theta_z + \frac{\theta_x\theta_y}{2} & 1 - \frac{\theta_x^2 + \theta_z^2}{2} & -\theta_x + \frac{\theta_y\theta_z}{2} \\ -\theta_y + \frac{\theta_x\theta_z}{2} & \theta_x + \frac{\theta_y\theta_z}{2} & 1 - \frac{\theta_x^2 + \theta_y^2}{2} \end{bmatrix} \tag{9}$$

Substituting this second order approximation for the rotation matrix into Eq. (8), one obtains the displacement vector components of a point P, in a given layer-k, as function of the displacements and rotations of the layer cross-section, referred to the local reference system r^k, in the form:

$$\begin{aligned} u_P^k &= u^k - y\theta_z^k + z\theta_y^k + y\frac{\theta_x^k\theta_y^k}{2} + z\frac{\theta_x^k\theta_z^k}{2} \\ v_P^k &= v - z\theta_x^k - y\frac{\theta_x^{k2} + \theta_z^{k2}}{2} + z\frac{\theta_y^k\theta_z^k}{2} \\ w_P^k &= \underbrace{w + y\theta_x^k}_{\text{Linear}} \underbrace{+ y\frac{\theta_y^k\theta_z^k}{2} - z\frac{\theta_x^{k2} + \theta_y^{k2}}{2}}_{\text{Non-Linear}} \end{aligned} \tag{10}$$

where: u_P^k, v_P^k and w_P^k are the displacements of point P, in the local reference system r^k of layer-k; u^k, θ_x^k, θ_y^k and θ_z^k are axial displacements and rotations measured at the geometric center of each

layer-k; v and w are the transverse displacements (assumed equal for all layers); and y and z are the local coordinates of point P, defined within layer-k thickness ($r_i^k \leqslant \sqrt{y^2+z^2} \leqslant r_o^k$), with r_i^k and r_o^k being the inner and outer radius, respectively.

The Green–Lagrange strain tensor components, used in the evaluation of the element strain energy, with the principle of virtual work (PVW) [19], is obtained from the displacements at a point P of any layer cross section as

$$\begin{aligned}
\varepsilon_{xx} &= \frac{\partial u_p}{\partial x} + \frac{1}{2}\left(\frac{\partial u_p}{\partial x}\right)^2 + \frac{1}{2}\left(\frac{\partial v_P}{\partial x}\right)^2 + \frac{1}{2}\left(\frac{\partial w_P}{\partial x}\right)^2 \\
\gamma_{xy} &= \frac{\partial u_P}{\partial y} + \frac{\partial v_P}{\partial x} + \frac{\partial u_P}{\partial x}\frac{\partial u_P}{\partial y} + \frac{\partial v_P}{\partial x}\frac{\partial v_P}{\partial y} + \frac{\partial w_P}{\partial x}\frac{\partial w_P}{\partial y} \\
\gamma_{xz} &= \underbrace{\frac{\partial u_P}{\partial z} + \frac{\partial w_P}{\partial x}}_{\text{Linear}(e_{ij})} + \underbrace{\frac{\partial u_P}{\partial x}\frac{\partial u_P}{\partial z} + \frac{\partial v_P}{\partial x}\frac{\partial v_P}{\partial z} + \frac{\partial w_P}{\partial x}\frac{\partial w_P}{\partial z}}_{\text{Non-Linear}(\eta_{ij})}
\end{aligned} \tag{11}$$

2.3. Finite element formulation

The multilayered element formulation is obtained considering the contribution of each layer – associated to linear and nonlinear strain contributions – and straining at each interface material between layers. Considering the equilibrium of a single element layer at time $(t + \Delta t)$, the PVW for updated Lagrangian formulation, gives [19]:

$$\int_V S_{ij}^{t+\Delta t}\delta\varepsilon_{ij}^{t+\Delta t}\,dV = \Re^{t+\Delta t} \tag{12}$$

where $S_{ij}^{t+\Delta t}$ is the second Piola–Kirchoff tensor [20]; $\varepsilon_{ij}^{t+\Delta t}$ is the Green–Lagrange strain tensor [20]; and $\Re^{t+\Delta t}$ is the virtual work due to external loading (body and surface forces), given by:

$$\Re^{t+\Delta t} = \sum_i \left(\int_V f_i^{B(t+\Delta t)}\delta u_i\,dV + \int_S f_i^{S(t+\Delta t)}\delta u_i\,dS\right) \tag{13}$$

with $f_i^{B(t+\Delta t)}$ and $f_i^{S(t+\Delta t)}$ being body and surface force components, respectively; and δu_i is the virtual displacement vector component.

Variables in Eq. (12) are accounted from the configuration C_{ref} shown in Fig. 1. Linearized incremental equation requires small displacement increments, therefore, the second Piola–Kirchoff stress and the Green–Lagrange strain tensor components can be written in incremental form as

$$S_{ij}^{t+\Delta t} = \tau_{ij}^t + \Delta\tau_{ij} \quad \text{and} \quad \varepsilon_{ij}^{t+\Delta t} = \varepsilon_{ij}^t + \Delta\varepsilon_{ij} \tag{14}$$

where τ_{ij}^t are known Cauchy stress tensor components; $\Delta\tau_{ij}$ are the incremental stress components; ε_{ij}^t are the known Cauchy–Green strain tensor components; and $\Delta\varepsilon_{ij}$ are the incremental strains, which are obtained from Eq. (11) by using the incremental displacements. Thus, Eq. (12) can be rewritten as follows:

$$\int_V (\tau_{ij}^t + \Delta\tau_{ij})\delta(\varepsilon_{ij}^t + \Delta\varepsilon_{ij})\,dV = \Re^{t+\Delta t} \tag{15}$$

In the reference configuration the element is subjected to rigid body motions only, i.e., there is no deformation, so $\delta\varepsilon_{ij}^t = 0$. Thus, Eq. (15) turns:

$$\int_V \Delta\tau_{ij}\delta\Delta\varepsilon_{ij}\,dV + \int_V \tau_{ij}^t\delta\Delta\varepsilon_{ij}\,dV = \Re^{t+\Delta t} \tag{16}$$

The incremental stresses $(\Delta\tau_{ij})$ are obtained from the incremental strains $(\Delta\varepsilon_{ij})$ by using a suitable constitutive relation:

$$\Delta\tau_{ij} = C_{ijkl}\Delta\varepsilon_{kl} \tag{17}$$

where C_{ijkl} is the material constitutive tensor.

As shown in Eq. (11), the incremental strains have linear (Δe_{ij}) and nonlinear $(\Delta\eta_{ij})$ terms, i.e.:

$$\Delta\varepsilon_{ij} = \Delta e_{ij} + \Delta\eta_{ij} \tag{18}$$

Assuming a linear approximation for the incremental stresses and strains, one obtains:

$$\Delta\tau_{ij} = C_{ijkl}\Delta e_{kl} \quad \text{and} \quad \delta\Delta\varepsilon_{ij} = \delta\Delta e_{ij} \tag{19}$$

Substituting Eqs. (18) and (19) into Eq. (16), one obtains the following linearized equation:

$$\begin{aligned}
&\underbrace{\int_V C_{ijkl}\Delta e_{kl}\delta\Delta e_{ij}\,dV}_{\text{Linear}} + \underbrace{\int_V \tau_{ij}^t\delta\Delta\eta_{ij}\,dV}_{\text{Nonlinear}} \\
&= \underbrace{\Re^{t+\Delta t}}_{\text{External Forces}} - \underbrace{\int_V \tau_{ij}^t\delta\Delta e_{ij}\,dV}_{\text{Internal Forces}}
\end{aligned} \tag{20}$$

In this equation, the left hand side leads to the linear and nonlinear stiffness matrices and the right hand side leads to the external and internal force vectors.

2.4. Element displacement field interpolation

For a given layer, displacements within the element are obtained from interpolated nodal displacements using Hermite polynomials [19], which represent straight-beam linear solutions under constant normal, transverse shear and torsional internal loadings, under Euler–Bernoulli beam assumptions. Thus, the displacement field at layer-k is:

$$\begin{aligned}
u^k &= \underbrace{\left(1-\frac{\xi}{\ell}\right)u_1^k + \frac{\xi}{\ell}u_2^k}_{u_0^k} + \underbrace{\frac{6\phi_1}{\ell}y v_1 - \frac{6\phi_1}{\ell}y v_2}_{-\frac{dv_0}{d\xi}y} + \underbrace{\frac{6\phi_1}{\ell}z w_1 - \frac{6\phi_1}{\ell}z w_2}_{-\frac{dw_0}{d\xi}z} \\
&\quad + \underbrace{\phi_2 z\theta_{y_1}^k - \phi_3 z\theta_{y_2}^k}_{\theta_y^k z} + \underbrace{(-\phi_2 y\theta_{z_1}^k + \phi_3 y\theta_{z_2}^k)}_{-\theta_z^k y} + \underbrace{(1-6\phi_1)z\beta_1^k + (1-6\phi_1)y\beta_2^k}_{\beta_1^k \text{ and } \beta_2^k \text{ constants in } \xi} \\
v^k &= \underbrace{\phi_4 v_1 + \phi_6 v_2}_{v_0} + \underbrace{\left(-\left(1-\frac{\xi}{\ell}\right)z\theta_{x_1}^k - \frac{\xi}{\ell}z\theta_{x_2}^k\right)}_{-\theta_x^k z} + \underbrace{\phi_5\ell\theta_{z_1}^k - \phi_1\xi\theta_{z_2}^k}_{-\overline{v}^k} + (\xi-\phi_7\ell)\beta_2^k \\
w^k &= \underbrace{\phi_4 w_1 + \phi_6 w_2}_{w_0} + \underbrace{\left(1-\frac{\xi}{\ell}\right)y\theta_{x_1}^k + \frac{\xi}{\ell}y\theta_{x_2}^k}_{\theta_x^k y} + \underbrace{(-\phi_5\ell\theta_{y_1}^k + \phi_1\xi\theta_{y_2}^k)}_{\overline{w}^k} + (\xi-\phi_7\ell)\beta_1^k
\end{aligned} \tag{21}$$

where u_0^k is the axial displacements of the element centerline at layer-k; ξ is the longitudinal coordinate along element; v_0 and w_0 are transverse displacements at the element centerline; $\overline{v}^k$ and $\overline{w}^k$ are transverse displacements along the layer-k centerline due to the nodal rotations θ_z^k and θ_y^k, respectively; and β_1^k and β_2^k are shear strains at planes $(\xi$–$y)$ and $(\xi$–$z)$, respectively (assumed constant along element length); and ϕ_i are the standard Hermite polynomials [19].

Eq. (21) can be extended to element coordinates at layer-k, in matrix form, as follows:

$$\left[u^k(\xi,y,z) \quad v^k(\xi,y,z) \quad w^k(\xi,y,z)\right]^T = \mathbf{H}^k(\xi,y,z)\mathbf{u}^k \tag{22}$$

where $u^k(\xi,y,z)$ $v^k(\xi,y,z)$ and $w^k(\xi,y,z)$ are the displacements at a point of local coordinates (ξ,y,z), at the element layer-k. The element interpolation matrix $\mathbf{H}^k(\xi,y,z)$ is obtained from Eq. (21) and is presented explicitly in Appendix B.1. The incremental displacement vector $\mathbf{u}^k$ (nodal translations and rotations) associated to element layer-k results in

$$\mathbf{u}^{kT} = \left[u_1^k \;\; v_1^k \;\; w_1^k \;\; \theta_{x_1}^k \;\; \theta_{y_1}^k \;\; \theta_{z_1}^k \;\; u_2^k \;\; v_2^k \;\; w_2^k \;\; \theta_{x_2}^k \;\; \theta_{y_2}^k \;\; \theta_{z_2}^k \;\; \beta_1^k \;\; \beta_2^k\right] \tag{23}$$

Each linear strain component in Eq. (11), obtained from the displacements given by Eq. (21), are defined at any point of layer-k by:

$$e_{xx}^k = \frac{du^k}{d\xi} = \frac{du_0^k}{d\xi} - \frac{d^2 v_0}{d\xi^2} y - \frac{d^2 w_0}{d\xi^2} z + \frac{d\theta_y^k}{d\xi} z - \frac{d\theta_z^k}{d\xi} y - 6\frac{d\phi_1}{d\xi}\beta_1^k z - 6\frac{d\phi_1}{d\xi}\beta_2^k y \tag{24}$$

or

$$e_{xx}^k = -\frac{1}{\ell}u_1^k + \frac{6y}{\ell}\frac{d\phi_1}{d\xi}v_1 + \frac{6z}{\ell}\frac{d\phi_1}{d\xi}w_1 + z\frac{d\phi_2}{d\xi}\theta_{y_1}^k - y\frac{d\phi_2}{d\xi}\theta_{z_1}^k + \frac{1}{\ell}u_2^k - \frac{6y}{\ell}\frac{d\phi_1}{d\xi}v_2 - \frac{6z}{\ell}\frac{d\phi_1}{d\xi}w_2 - z\frac{d\phi_3}{d\xi}\theta_{y_2}^k + y\frac{d\phi_3}{d\xi}\theta_{z_2}^k - 6z\frac{d\phi_1}{d\xi}\beta_1^k - 6y\frac{d\phi_1}{d\xi}\beta_2^k \tag{25}$$

Similarly, the linear shear strain components e_{xy}^k and e_{xz}^k are:

$$2e_{xy}^k = \frac{du^k}{dy} + \frac{dv}{d\xi} = \left(-\frac{dv_0}{d\xi} - \theta_z^k + (1-6\phi_1)\beta_2^k\right) + \left(\frac{dv_0}{d\xi} - \frac{d\theta_x^k}{d\xi}z - \frac{d\overline{v}^k}{d\xi} + \left(1 - \frac{d\phi_7}{d\xi}\ell\right)\beta_2^k\right) \tag{26}$$

or

$$2e_{xy}^k = \frac{z}{\ell}\theta_{x_1}^k + \left(\ell\frac{d\phi_5}{d\xi} - \phi_2\right)\theta_{z_1}^k - \frac{z}{\ell}\theta_{x_2}^k + \left(\phi_3 - \phi_1 - \frac{d\phi_1}{d\xi}\xi\right)\theta_{z_2}^k + \left(2 - 6\phi_1 - \frac{d\phi_7}{d\xi}\ell\right)\beta_2^k \tag{27}$$

and,

$$2e_{xz}^k = \frac{du^k}{dz} + \frac{dw}{d\xi} = \left(-\frac{dw_0}{d\xi} + \theta_y^k + (1-6\varphi_1)\beta_1^k\right) + \left(\frac{dw_0}{d\xi} + \frac{d\theta_x^k}{d\xi}y + \frac{d\overline{w}^k}{d\xi} + \left(1 - \frac{d\varphi_7}{d\xi}\ell\right)\beta_1^k\right) \tag{28}$$

or

$$2e_{xz}^k = -\frac{y}{\ell}\theta_{x_1}^k + \left(\phi_2 - \ell\frac{d\phi_5}{d\xi}\right)\theta_{y_1}^k + \frac{y}{\ell}\theta_{x_2}^k + \left(\phi_1 - \phi_3 + \xi\frac{d\phi_1}{d\xi}\right)\theta_{y_2}^k + \left(2 - 6\phi_1 - \ell\frac{d\phi_7}{d\xi}\right)\beta_1^k \tag{29}$$

Thus, from Eqs. (25), (27), and (29), linear strain components results in the following matrix form

$$\mathbf{e} = \begin{bmatrix} e_{xx}^k & 2e_{xy}^k & 2e_{xz}^k \end{bmatrix}^T = \mathbf{B}_L^k \mathbf{u}^k \quad \text{and} \quad \delta\mathbf{e} = \mathbf{B}_L^k \delta\mathbf{u}^k \tag{30}$$

where $\mathbf{B}_L^k$ is the linear compatibility matrix for layer-k, as defined in Appendix B.2.

Similarly, for the nonlinear term in Eq. (20) the following matrix form is used:

$$\tau_{ij}\delta\Delta\eta_{ij} = \delta\mathbf{u}^{k^T}\mathbf{B}_G^{k^T}\boldsymbol{\tau}\mathbf{B}_G^k\mathbf{u}^k \tag{31}$$

where $\mathbf{B}_G^k$ is the nonlinear (geometric) compatibility matrix for layer-k, as defined in Appendix B.3, and:

$$\boldsymbol{\tau}^k = \begin{bmatrix} \tau_{xx}^k & 0 & 0 & \tau_{xy}^k & 0 & \tau_{xz}^k & 0 \\ 0 & \tau_{xx}^k & 0 & 0 & 0 & 0 & \tau_{xz}^k \\ 0 & 0 & \tau_{xx}^k & 0 & \tau_{xy}^k & 0 & 0 \\ \tau_{xy}^k & 0 & 0 & 0 & 0 & 0 & 0 \\ 0 & 0 & \tau_{xy}^k & 0 & 0 & 0 & 0 \\ \tau_{xz}^k & 0 & 0 & 0 & 0 & 0 & 0 \\ 0 & \tau_{xz}^k & 0 & 0 & 0 & 0 & 0 \end{bmatrix} \tag{32}$$

Stress components, at each element layer-k, in local coordinates, are obtained from the beam internal forces, at the element nodes, as indicated below.

$$\begin{aligned} \tau_{xx}^k &= \tfrac{N^k}{A^k} + \tfrac{M_y^k}{I^k}z - \tfrac{M_z^k}{I^k}y \\ \tau_{xy}^k &= -\tfrac{M_x^k}{J^k}z + \tfrac{V_y^k}{A^k} \\ \tau_{xz}^k &= \tfrac{M_x^k}{J^k}y + \tfrac{V_z^k}{A^k} \end{aligned} \quad , \quad \text{with :} \quad \begin{aligned} N^k &= -F_1^k \\ V_y^k &= -F_2^k \\ V_z^k &= -F_3^k \\ M_x^k &= -F_4^k \\ M_y^k &= F_3^k\xi + F_5^k \\ M_z^k &= -F_2^k\xi + F_6^k \end{aligned} \tag{33}$$

where F_i^k are the layer-k vector of internal forces and moments components; A^k is the layer-k cross section area; I^k is the layer-k cross section moment of inertia with respect to the axis of symmetry; $J^k = 2I^k$ is the layer-k cross section polar moment of inertia with respect to the geometric center; and ξ is the local coordinate along element length. Details on the derivations of the geometric compatibility matrix ($\mathbf{B}_G^k$) and the stress components matrix ($\boldsymbol{\tau}^k$) are presented in Bathe and Bolourchi [15].

2.5. Element layer stiffness matrices

For a given layer-k, the element linear stiffness matrix is obtained by substituting Eq. (30) in the first term of Eq. (20):

$$\mathbf{K}_L^k = \int_0^\ell \int_{r_i^k}^{r_o^k} \int_0^{2\pi} r\mathbf{B}_L^{k^T}\mathbf{C}^k\mathbf{B}_L^k\, d\varphi\, dr\, d\xi \tag{34}$$

where $\mathbf{B}_L$ is the linear compatibility matrix, as defined in Appendix B.2, using $y = r\cos\phi$ and $z = r\sin\phi$, and

$$\mathbf{C}^k = \begin{bmatrix} E^k & 0 & 0 \\ 0 & G^k & 0 \\ 0 & 0 & G^k \end{bmatrix} \tag{35}$$

The geometric stiffness matrix contribution of each layer ($\mathbf{K}_G^k$) is obtained from Eq. (31) and the second term of Eq. (20) that results in

$$\mathbf{K}_G^k = \int_0^\ell \int_{r_i^k}^{r_o^k} \int_0^{2\pi} r\mathbf{B}_G^{k^T}\boldsymbol{\tau}^k\mathbf{B}_G^k\, d\varphi\, dr\, d\xi \tag{36}$$

Appendices B.5 and B.6 present ($\mathbf{K}_L^k$) and ($\mathbf{K}_G^k$) matrices explicitly.

2.6. Contact conditions

In this section, the model solutions for the interlayer contact used in the finite element formulation are derived. The longitudinal and circumferential relative displacements between layers results in shear stresses at the interlayer material, as shown in Fig. 4. In the model each interface is assumed under constant (through the thickness) shearing straining as its thickness (h) is very small when compared to other pipe cross section dimensions.

Thus, shear strain and stress at interface are evaluated using the following linear approximation:

$$\gamma = \frac{\Delta u}{h} \quad \text{and} \quad \tau = G\gamma = \frac{G}{h}\Delta u = k\overline{\gamma} \tag{37}$$

where G is the interface material shear modulus; $k = G/h$ is the overall contact stiffness; and $\overline{\gamma} = \Delta u$ is the interlayer relative displacement.

The idea behind this proposal is to employ material constitutive relations that may represent the overall physical meaning of contact conditions at the interface material including certain damage conditions. These attempts are described as follows:

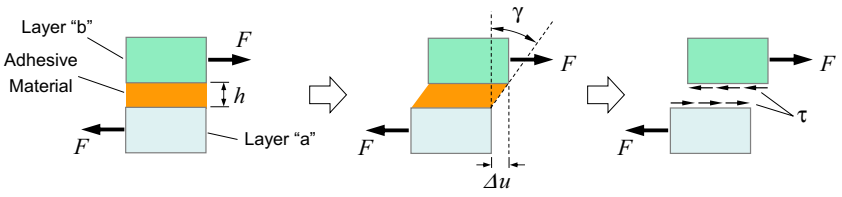

Fig. 4. Details of interface straining in a two-layer pipe wall segment.

A. Linear elastic slip

In this case the interlayer material behaves according to the constitutive relation shown in Fig. 5. Contact stress is proportional to the layers relative displacement. This constitutive relation is represented by the linear model solution where total strain energy in the adhesive is preserved after unloading.

B. Slip with static friction

In this case rupture occurs when shear stress in adhesive material reaches a limit value τ_ℓ. Thereafter, contact condition between layers remains through friction (static) forces and the "material law" follows the bi-linear constitutive relation shown in Fig. 6. In a cycle loading process, total strain energy at interface material is not preserved.

C. Slip with kinetic friction

In this case a multi-linear constitutive model is required to represent material rupture but with kinetic friction between layers. After reaching a limit value, shear stress drops to a lower value keeping it constant as in kinetic friction force fashion. Again, as in the previous case, total potential energy in the adhesive is partially preserved.

D. Rupture

In this case, a multi-linear constitutive model is employed to represent material rupture with no friction between layers. Thus, after reaching a limit value, shear stress at interface vanishes. By this model, in a cycling loading process, the total strain energy stored during the interface linear behavior is completely lost.

2.7. Interface constitutive model

In this section, the nonlinear constitutive relations shown in Figs. 6–8 for the interface material, is presented in detail. For simplicity, the models presented above are one-dimensional. However, in a multi-layered pipe, the relative displacements can occur in the axial ($\overline{\gamma}_x$) as circumferential ($\overline{\gamma}_\varphi$) directions, as shown in Fig. 9.

For all contact conditions discussed, stress state at the interface material must remain within the following domain

$$\mathbf{D}_\tau = \{\boldsymbol{\tau} \in \mathbf{R} | f(\boldsymbol{\tau}, \alpha) \leq 0\} \tag{38}$$

where $f(\boldsymbol{\tau}, \alpha)$ is the associated yield-type function, expressed in terms of the contact stresses $\boldsymbol{\tau}$ and hardening parameter α, with:

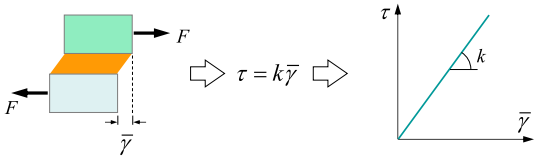

Fig. 5. Linear elastic constitutive relation – slip model representation.

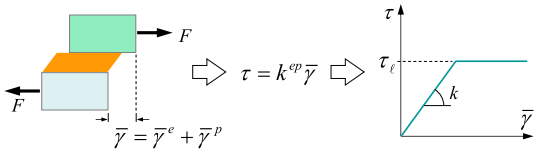

Fig. 6. Layer contact with static friction.

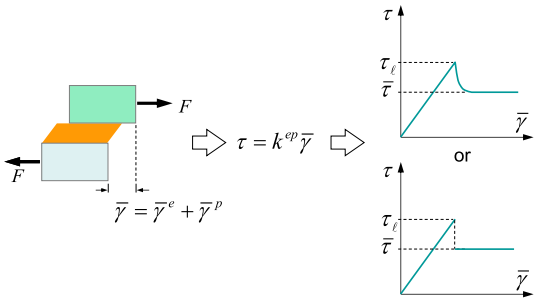

Fig. 7. Layer contact with kinetic friction.

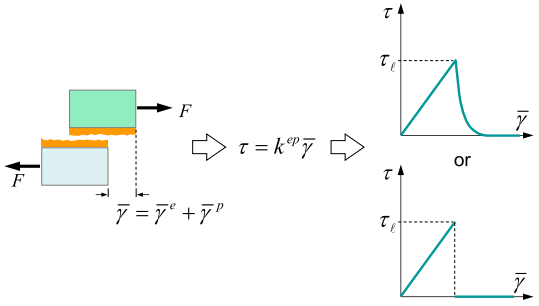

Fig. 8. Rupture – multi-linear elastic-perfect plastic model.

$$\boldsymbol{\tau} = \begin{bmatrix} \tau_x & \tau_\varphi \end{bmatrix}^T \tag{39}$$

The choice of an appropriate yield function defines the slip condition model. Table 1 presents the corresponding yield function used to represent each of the contact conditions studied in this work, as discussed in Section 2.6.

where $|\boldsymbol{\tau}| = \sqrt{\tau_x^2 + \tau_\varphi^2}$; with τ_x and τ_φ being the contact stresses in the axial and circumferential directions as shown in Fig. 9; and τ_ℓ is the limit contact stress.

According to Simo and Hughes [21], the nonlinear slip model can be characterized by means of the following set of equations

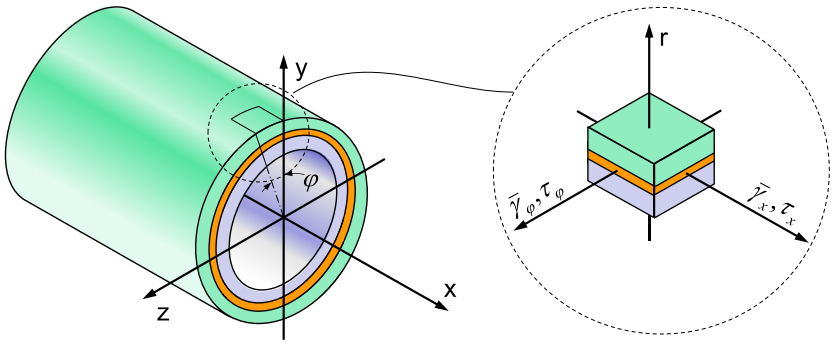

Fig. 9. Directions for relative displacements.

Table 1
Slip model conditions.

Slip model	Yielding function	H
A. Linear elastic slip	Not applicable	–
B. Slip in static friction (bi-linear)	$f(\boldsymbol{\tau}) = \lvert\boldsymbol{\tau}\rvert - \tau_\ell$	0
C. Slip in kinetic friction (multi-linear)	$f(\boldsymbol{\tau}, \alpha) = \lvert\boldsymbol{\tau}\rvert - \tau_\ell(\alpha)$	According to the hardening law
D. Rupture (multi-linear)		

$$\begin{aligned}
&\overline{\boldsymbol{\gamma}} = \overline{\boldsymbol{\gamma}}^e + \overline{\boldsymbol{\gamma}}^{in}\\
&\boldsymbol{\tau} = k\overline{\boldsymbol{\gamma}}^e = k(\overline{\boldsymbol{\gamma}} - \overline{\boldsymbol{\gamma}}^{in})\\
&d\overline{\boldsymbol{\gamma}}^{in} = \lambda\mathbf{r} = \lambda\frac{df}{d\boldsymbol{\tau}}\\
&d\alpha = \lambda
\end{aligned} \tag{40}$$

where $\overline{\boldsymbol{\gamma}}$, $\overline{\boldsymbol{\gamma}}^e$ and $\overline{\boldsymbol{\gamma}}^{in}$ are the vectors of total, elastic and inelastic slip measures obtained from relative longitudinal and circumferential relative displacements between layers; $\boldsymbol{\tau}$ is the vector of contact stresses; k is the elastic contact stiffness parameter; α is the hardening parameter; λ is the inelastic slip increment to be determined; and $\mathbf{r}$ is a unit vector that indicates the "yield" direction given by:

$$\mathbf{r} = \frac{1}{|\boldsymbol{\tau}|}\begin{bmatrix}\tau_x\\ \tau_\varphi\end{bmatrix} \tag{41}$$

Thus, the associated mathematical problem consists in: given $\{\overline{\boldsymbol{\gamma}}_n, \overline{\boldsymbol{\gamma}}_n^{in}, \boldsymbol{\tau}_n, \alpha_n\}$ and $\overline{\boldsymbol{\gamma}}_{n+1}$ as a known solution state and new relative displacements, respectively, obtain $\overline{\boldsymbol{\gamma}}_{n+1}^{in}$, α_{n+1} and $\boldsymbol{\tau}_{n+1}$. This problem is solved in two steps. First, an elastic increment is assumed to obtain the following trial state

$$\begin{aligned}
&\boldsymbol{\tau}_{n+1}^* = k(\overline{\boldsymbol{\gamma}}_{n+1} - \overline{\boldsymbol{\gamma}}_n^{in}) \equiv \boldsymbol{\tau}_n + k\Delta\overline{\boldsymbol{\gamma}}_n\\
&\overline{\boldsymbol{\gamma}}_{n+1}^{in*} = \overline{\boldsymbol{\gamma}}_n^{in}\\
&\alpha_{n+1}^* = \alpha_n\\
&f_{n+1}^* = |\boldsymbol{\tau}_{n+1}^*| - \tau_{\ell_n}
\end{aligned} \tag{42}$$

From the trial state, it is possible to determine if the increment of slip is elastic or inelastic according to the criterion

$$f_{n+1}^*\begin{cases}\leq 0 & \Rightarrow \text{ elastic increment} \quad \lambda = 0\\ > 0 & \Rightarrow \text{ inelastic increment} \quad \lambda > 0\end{cases} \tag{43}$$

Assuming an inelastic increment, one obtains the stress $\boldsymbol{\tau}_{n+1}$ in terms of the trial stress $\boldsymbol{\tau}_{n+1}^*$ and the inelastic slip modulus λ as:

$$\begin{aligned}
\boldsymbol{\tau}_{n+1} &= k(\overline{\boldsymbol{\gamma}}_{n+1} - \overline{\boldsymbol{\gamma}}_{n+1}^{in}) = k(\overline{\boldsymbol{\gamma}}_{n+1} - \overline{\boldsymbol{\gamma}}_n^{in}) - k(\overline{\boldsymbol{\gamma}}_{n+1}^{in} - \overline{\boldsymbol{\gamma}}_n^{in})\\
&= \boldsymbol{\tau}_{n+1}^* - k\lambda\mathbf{r}_{n+1}
\end{aligned} \tag{44}$$

Therefore, since $\lambda > 0$, the actual state is written as

$$\begin{aligned}
&\boldsymbol{\tau}_{n+1} = \boldsymbol{\tau}_{n+1}^* - k\lambda\mathbf{r}_{n+1}\\
&\overline{\boldsymbol{\gamma}}_{n+1}^{in} = \overline{\boldsymbol{\gamma}}_n^{in} + \lambda\mathbf{r}_{n+1}\\
&\alpha_{n+1} = \alpha_n + \lambda\\
&f_{n+1} = |\boldsymbol{\tau}_{n+1}| - \tau_{\ell_{n+1}} = 0
\end{aligned} \tag{45}$$

Now the above problem is solved explicitly in terms of the trial elastic state by the following procedure:

$$|\boldsymbol{\tau}_{n+1}|\mathbf{r}_{n+1} = |\boldsymbol{\tau}_{n+1}^*|\mathbf{r}_{n+1}^* - k\lambda\mathbf{r}_{n+1} \tag{46}$$

Collecting terms in Eq. (46), one obtains

$$[|\boldsymbol{\tau}_{n+1}| + k\lambda]\mathbf{r}_{n+1} = |\boldsymbol{\tau}_{n+1}^*|\mathbf{r}_{n+1}^* \tag{47}$$

As $\lambda > 0$ and $k > 0$, the term within brackets in Eq. (47) is necessarily positive. Therefore it is required that

$$\mathbf{r}_{n+1} = \mathbf{r}_{n+1}^* \tag{48}$$

along with the condition

$$|\boldsymbol{\tau}_{n+1}| + k\lambda = |\boldsymbol{\tau}_{n+1}^*| \tag{49}$$

From Eqs. (45) and (49), the yield criterion f_{n+1} is written as

$$f_{n+1} = |\boldsymbol{\tau}_{n+1}^*| - k\lambda - \tau_\ell(\alpha_n + \lambda) = 0 \tag{50}$$

Depending on the hardening law $\tau_\ell(\alpha_n + \lambda)$, Eq. (50) can be nonlinear and must be solved numerically for λ. The inelastic constitutive relation is then obtained from the consistency condition ($\lambda\, df = 0$), as described in Simo and Hughes [21]. If $\lambda > 0$, then

$$df(\boldsymbol{\tau}, \alpha) = \frac{df}{d\boldsymbol{\tau}}d\boldsymbol{\tau} + \frac{df}{d\alpha}d\alpha = 0 \tag{51}$$

Substituting values for $df/d\boldsymbol{\tau}$, $df/d\alpha$, $d\boldsymbol{\tau}$ and $d\alpha$, one obtains

$$\mathbf{r}^{\mathbf{T}}k(d\overline{\boldsymbol{\gamma}} - \lambda\mathbf{r}) - \lambda H = 0 \tag{52}$$

where $H = df/d\alpha$ is set for each hardening law, as shown in Table 1 .

Solving Eq. (52) for λ, one obtains

$$\lambda = \frac{k\mathbf{r}}{k + H}d\overline{\boldsymbol{\gamma}} \tag{53}$$

that substituted into the rate form of the elastic relationship given by the second Eq. (40), yields

$$d\boldsymbol{\tau} = \frac{kH}{k+H} d\overline{\boldsymbol{\gamma}} \tag{54}$$

Therefore,

$$d\boldsymbol{\tau} = k^{ep}\, d\overline{\boldsymbol{\gamma}} \tag{55}$$

where

$$k^{ep} = \begin{cases} k & \text{if } \lambda = 0 \\ \frac{kH}{k+H} & \text{if } \lambda > 0 \end{cases} \tag{56}$$

2.8. Interface stiffness matrix

At the interface, adhesive material is assumed under constant pure shear deformation, throughout the cross-section thickness. Interface contribution to the element stiffness matrix is obtained by considering the strain energy associated to the interface material due to adjoining layers relative displacements ($\overline{\gamma}_l$), which denotes the equivalent shear strains. These are due to axial and torsional displacements between layers (say layers k and $k+1$), and an equivalent strain vector is defined with two components:

$$\overline{\boldsymbol{\gamma}}_i^k = \begin{bmatrix} \overline{\gamma}_x^k & \overline{\gamma}_\varphi^k \end{bmatrix}^T \tag{57}$$

with

$$\begin{aligned} \overline{\gamma}_x^k(\varphi) &= (u^{k+1}(\varphi) - u^k(\varphi)) \\ \overline{\gamma}_\varphi^k &= r(\theta_x^{k+1} - \theta_x^k) \end{aligned} \tag{58}$$

where $u^k(\varphi)$ and θ_x^k are the longitudinal displacement and torsional rotation of layer-k cross section, respectively; and φ is the angular coordinate at the interface cross section, as shown in Fig. 10.

For a linearly elastic model, the constitutive relation at the interface material above layer-k results in

$$\boldsymbol{\tau}_i^k = \begin{bmatrix} \tau_x^k \\ \tau_\varphi^k \end{bmatrix} = \begin{bmatrix} k_c^k & 0 \\ 0 & k_c^k \end{bmatrix} \begin{bmatrix} \overline{\gamma}_x^k \\ \overline{\gamma}_\varphi^k \end{bmatrix} = k_c^k \mathbf{I} \begin{bmatrix} \overline{\gamma}_x^k \\ \overline{\gamma}_\varphi^k \end{bmatrix} \tag{59}$$

where k_c^k is associated to contact stiffness between layers k and $k+1$; and τ_x^k and τ_φ^k are contact stress components along the longitudinal and circumferential directions, respectively.

Slip condition between layers is modeled by imposing a limit value on the shear stress (τ_ℓ) at the interface material, as described in Section 2.6. This is obtained by using a suitable constitutive model, according to one of the yield-type functions presented in Table 1, in Section 2.7. Thus, the constitutive relation for interface k results in

$$\boldsymbol{\tau}_i^k = k_c^{ep} \mathbf{I} \overline{\boldsymbol{\gamma}}_i^k \tag{60}$$

where $\boldsymbol{\tau}_i^k$ and $\overline{\boldsymbol{\gamma}}_i^k$ are as in Eqs. (59) and (57), respectively; and the nonlinear slip modulus (k_c^{ep}) is obtained from Eq. (56).

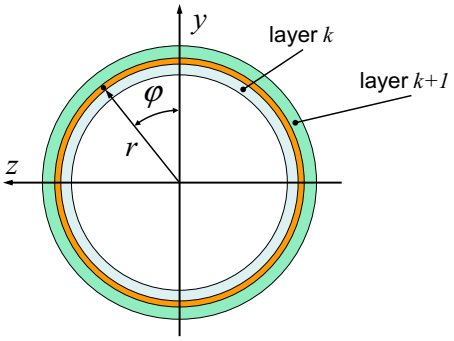

Fig. 10. Angular coordinate φ at the interface.

Thus, considering the strain energy due to shearing at the interface material, one obtains

$$\pi_{\tau_i}^k = \frac{1}{2} \int_S \boldsymbol{\tau}_i^{kT} \overline{\boldsymbol{\gamma}}^k \, dS \tag{61}$$

Substitution of the expressions for $\boldsymbol{\tau}_i^k$ and $\overline{\boldsymbol{\gamma}}^k$ leads to

$$\pi_{\tau_i}^k = \frac{1}{2} \int_0^\ell \int_0^{2\pi} k_c^{ep} r((u^{k+1} - u^k)^2 + r^2(\theta_x^{k+1} - \theta_x^k)^2)\, d\varphi\, d\xi \tag{62}$$

The variation of the interface strain energy is:

$$\begin{aligned} \delta\pi_{\tau_i}^k = \int_0^\ell \int_0^{2\pi} & k_c^{ep} r((u^{k+1} - u^k)\delta(u^{k+1} - u^k) \\ & + r^2(\theta_x^{k+1} - \theta_x^k)\delta(\theta_x^{k+1} - \theta_x^k))\, d\varphi\, d\xi \end{aligned} \tag{63}$$

which can be rewritten in the following compact matrix form

$$\delta\pi_{\tau_i}^k = \delta\mathbf{u} \left(\int_0^\ell \int_0^{2\pi} r \mathbf{B}_i^{kT} k_c^{ep} \mathbf{B}_i^k \, d\varphi\, d\xi \right) \mathbf{u} \tag{64}$$

The stiffness matrix associated to each interface material between layers is

$$\mathbf{K}_i^k = \int_0^\ell \int_0^{2\pi} r \mathbf{B}_i^{kT} k_c^{ep} \mathbf{B}_i^k \, d\varphi\, d\xi \tag{65}$$

where $\mathbf{B}_i^k$ is the interface compatibility matrix, defined in Appendix B.4. The incremental displacement vector, for element interface k, in the local element system is given by

$$\mathbf{u}^{kT} = \begin{bmatrix} u_1^k & \theta_{x_1}^k & \theta_{y_1}^k & \theta_{z_1}^k & u_2^k & \theta_{x_2}^k & \theta_{y_2}^k & \theta_{z_2}^k & u_1^{k+1} & \theta_{x_1}^{k+1} \\ \theta_{y_1}^{k+1} & \theta_{z_1}^{k+1} & u_2^{k+1} & \theta_{x_2}^{k+1} & \theta_{y_2}^{k+1} & \theta_{z_2}^{k+1} & \beta_1^k & \beta_2^k & \beta_1^{k+1} & \beta_2^{k+1} \end{bmatrix} \tag{66}$$

In a linear-elastic slip model, with no damage in the interface material, the stiffness matrix is obtained analytically, as shown in Appendix B.7. However, in models with slip condition between layers, the stiffness matrix is obtained from the integral form in Eq. (65), which must be solved numerically.

2.9. Transverse displacement compatibility

At any spatial configuration, all element layers share the same axis, allowing slip between layers in axial and circumferential directions only, but requiring compatible transverse displacements. In the present work, this constraint condition is applied by using the penalty method for simplicity, considering equality constraints. By this method, two degrees-of-freedom are physically linked through an elastic member, with the constraint condition being imposed numerically. The choice of the appropriate value for the elastic constant relies on a numerical trial procedure. Thus, if any two degrees-of-freedom (u_i and u_j) are linked by a spring of stiffness k^p, the strain energy (due to the relative displacement), to be added to the variational indicator of the problem, is given by

$$\pi^* = \frac{1}{2} \int_u k^p (u_j - u_i)^2 \, du \tag{67}$$

The choice of the penalty parameter k^p is generally left to numerical investigation. In the present study, this parameter has been taken to be equal to the largest numerical value amongst all terms in the element stiffness matrix.

For the multilayer pipe beam element, the transverse degrees-of-freedom constraints between any layer (k) and the reference layer ($k = 1$) are obtained by using the following penalty matrix

$$\mathbf{K}_p^k = k^p \begin{bmatrix} \overline{\mathbf{k}}^p & \mathbf{0} \\ \mathbf{0} & \overline{\mathbf{k}}^p \end{bmatrix}, \quad \text{with} : \overline{\mathbf{k}}^p = \begin{bmatrix} 1 & 0 & -1 & 0 \\ 0 & 1 & 0 & -1 \\ -1 & 0 & 1 & 0 \\ 0 & -1 & 0 & 1 \end{bmatrix} \tag{68}$$

which is associated to the following nodal incremental displacement vector:

$$\mathbf{u}_p^k = \begin{bmatrix} v_1^1 & w_1^1 & v_1^k & w_1^k & v_2^1 & w_2^1 & v_2^k & w_2^k \end{bmatrix}^T \tag{69}$$

Special attention must be given to the transformations applied to the penalty matrix, as it must be computed in the nodal reference system. As shown in Fig. 11, for two initially aligned elements, in the element system, the penalty stiffness at the adjoining node of adjacent elements "1" and "2" are applied in different directions. To overcome this difficulty nodal reference system is used and, in this case, stiffness contributions from both elements are applied in a unique direction.

2.10. Element stiffness matrix

The multilayered pipe beam element can be considered as "fully bonded" or "unbonded", depending on the type of interaction between layers. For the unbonded element case, the stiffness matrix ($\mathbf{K}_e$) is obtained by the regular FEM assembling process, accounting for the influence of each layer and interfaces. The element penalty matrix ($\mathbf{K}_p$) is referred to each node reference system and is obtained by using the same procedure. After the assembly process, the element stiffness matrix ($\mathbf{K}_e$) is of order $14n_{layers} \times 14n_{layers}$. In the fully bonded condition, there is no contribution of interface and penalty matrices, and the element matrix is obtained by simply adding all layer matrices. In this case the element matrix dimension is 14×14. Eq. (70) shows both processes.

$$\left.\begin{aligned} &\mathbf{K}_{lay} = \mathop{\mathbf{A}}_{k=1}^{n_{layers}} (\mathbf{K}_L^k + \mathbf{K}_G^k) \\ &\mathbf{K}_{int} = \mathop{\mathbf{A}}_{k=1}^{n_{layers}-1} (\mathbf{K}_i^k) \\ &\mathbf{K}_e = \mathbf{K}_{lay} + \mathbf{K}_{int}; \quad \text{element reference system} \\ &\mathbf{K}_p = \mathop{\mathbf{A}}_{k=2}^{n_{layers}} (\mathbf{K}_p^k); \quad \text{nodal reference system} \end{aligned}\right\} \rightarrow \text{unbonded}$$

$$\mathbf{K}_e = \sum_{k=1}^{n_{layers}} (\mathbf{K}_L^k + \mathbf{K}_G^k) \qquad \rightarrow \text{fully bonded} \tag{70}$$

where $\mathbf{K}_{lay}$ is the element layers stiffness matrix; $\mathbf{K}_{int}$ is the element interfaces stiffness matrix; $\mathbf{K}_e$ is the element stiffness matrix including all layers and interfaces; $\mathbf{K}_p$ is the element penalty matrix; $\mathbf{A}$ stands for the assembly process.

In both cases, static condensation on the generalized degrees-of-freedom for shear strains is used to reduce matrix dimension. In this way, $\mathbf{K}_e$ matrix is partitioned as

$$\mathbf{K}_e = \begin{bmatrix} \mathbf{K}_{uu} & \mathbf{K}_{u\beta} \\ \mathbf{K}_{\beta u} & \mathbf{K}_{\beta\beta} \end{bmatrix} \tag{71}$$

and, by applying static condensation, the element stiffness matrix is obtained.

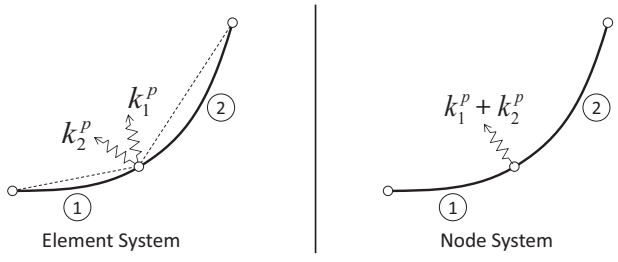

Fig. 11. Reference systems for penalty method.

3. Implementation of the three-dimensional multilayer element

The three-dimensional multilayered element has been implemented in a C++ code using object-oriented techniques, such as proposed by Lages et al. [22]. The program uses some of the algorithms presented by Leon et al. [23], to solve the resulting nonlinear equilibrium equations. Details of this implementation are presented in the following sections.

3.1. Global equilibrium equation

The present formulation includes large displacements and nonlinear constitutive relations within the interface material. Numerical solutions are obtained using an incremental procedure for equilibrium. The global dynamic equilibrium equation is presented in the following matrix form:

$$\mathbf{K}^i \Delta\mathbf{U} = \mathbf{R}^{i+1} - \mathbf{F}^i \tag{72}$$

where $\mathbf{K}$ is the structure global stiffness matrix, obtained from the elements matrices through an assemblage process; $\Delta\mathbf{U}$ is the global incremental displacements vector; $\mathbf{R}$ is the global external loading vector; and $\mathbf{F}$ is the structure global unbalanced internal forces vector.

A step-by-step procedure has been implemented considering

$$\mathbf{U}^{i+1} = \mathbf{U}^i + \Delta\mathbf{U} \tag{73}$$

where $\mathbf{U}^i$ is a known solution at iteration-i.

3.2. Element updating procedure

The nonlinear equilibrium equation, shown in Eq. (72), is solved by an iterative and incremental algorithm. Thus, at each equilibrium iteration, all stiffness matrices and internal force vectors, for each element, must be updated. In the following sections, the formulation for large displacements and rotations is presented. An updating procedure applied to all multilayered pipe beam element matrices is also detailed. It uses the element incremental displacements and rotations, obtained in the solution process at each iteration-i, to update all element reference systems. The procedure is performed according to the following steps:

1. Nodal positions and direction cosines of the element (straight axis direction) are updated from the incremental displacements ($\Delta\mathbf{u}^i$) obtained in the previous iteration;
2. Element and nodal transformation matrices are updated:
   2.1. Nodal rotation matrices ($\mathbf{R}_{n1}^{k(i)}$ and $\mathbf{R}_{n2}^{k(i)}$), for each layer, are updated from incremental rotations at each node: nodal incremental rotation matrices ($\mathbf{R}_{inc1}^{k(i)}$ and $\mathbf{R}_{inc2}^{k(i)}$) are obtained from the rotation increments using Eq. (2). Previous nodal rotation matrices are pre-multiplied by each of these matrices, i.e.,
   $$\mathbf{R}_{n1}^{k(i)} = \mathbf{R}_{inc1}^{k(i)} \mathbf{R}_{n1}^{k(i-1)} \quad \text{and} \quad \mathbf{R}_{n2}^{k(i)} = \mathbf{R}_{inc2}^{k(i)} \mathbf{R}_{n2}^{k(i-1)} \tag{74}$$
   2.2. The element transformation matrix ($\mathbf{R}_e^i$) is obtained from the straight element axis (defined by current nodal point positions) and from nodal rotation matrices: the first row in the element rotation matrix ($\mathbf{R}_e^i$) is given by the updated direction cosines of the element (vector $\mathbf{X}$); the second row (vector $\mathbf{Y}$) is given by averaging the second rows of the reference layer nodal matrices $\mathbf{R}_{n1}^{1(i)}$ (vector $\mathbf{y}_1^1$) and $\mathbf{R}_{n2}^{1(i)}$ (vector $\mathbf{y}_2^1$); and the third row (vector $\mathbf{Z}$) is obtained from the cross product between the first and second rows ($\mathbf{Z} = \mathbf{X} \times \mathbf{Y}$);
3. Relative displacements vectors ($\mathbf{u}_r^i$ and $\mathbf{u}_p^i$), in the local element and nodal reference systems, respectively, are then calculated.

3.1. Relative displacements between layers are obtained as follows:

3.1.1. First, the relative axial displacement of the reference layer (innermost layer) is computed subtracting its updated deformed length (ℓ^i) from element non-deformed length (ℓ_0):

$$\Delta\ell^i = \ell^i - \ell_0 \tag{75}$$

3.1.2. Then, nodal relative displacements between each layer (k) and the reference layer ($k = 1$) are computed in the global reference system. This must be done individually for each node:

$$\Delta\mathbf{u}_1^k = \mathbf{u}_1^k - \mathbf{u}_1^1 \text{ and } \Delta\mathbf{u}_2^k = \mathbf{u}_2^k - \mathbf{u}_2^1, \quad k = 2 \text{ to } N_{layers} \tag{76}$$

3.1.3. The nodal relative displacements for each layer are transferred to local element system and also to the nodal reference systems:

$$\begin{cases} \Delta\mathbf{u}_{e1}^k = \mathbf{R}_e^{(i)^T}\Delta\mathbf{u}_1^k \text{ and } \Delta\mathbf{u}_{e2}^k = \mathbf{R}_e^{(i)^T}\Delta\mathbf{u}_2^k \\ \Delta\mathbf{u}_{n1}^k = \mathbf{R}_{n1}^{(i)^T}\Delta\mathbf{u}_1^k \text{ and } \Delta\mathbf{u}_{n2}^k = \mathbf{R}_{n2}^{(i)^T}\Delta\mathbf{u}_2^k \end{cases} k = 2 \text{ to } N_{layers} \tag{77}$$

3.2. Nodal relative rotation between each layer and the straight axis of element are obtained from the nodal transformation matrices of each layer and from the element transformation matrix in the reference configuration. According to Crisfield [17], these rotations can be obtained from the expressions below

$$\begin{aligned} 2\sin(\Delta\theta_{1x}^k) &= -\mathbf{z}_1^k\mathbf{Y} + \mathbf{y}_1^k\mathbf{Z} & 2\sin(\Delta\theta_{2x}^k) &= -\mathbf{z}_2^k\mathbf{Y} + \mathbf{y}_2^k\mathbf{Z} \\ 2\sin(\Delta\theta_{1y}^k) &= -\mathbf{x}_1^k\mathbf{Z} + \mathbf{z}_1^k\mathbf{X} \quad \text{and} & 2\sin(\Delta\theta_{2y}^k) &= -\mathbf{x}_2^k\mathbf{Z} + \mathbf{z}_2^k\mathbf{X} \\ 2\sin(\Delta\theta_{1z}^k) &= -\mathbf{y}_1^k\mathbf{X} + \mathbf{x}_1^k\mathbf{Y} & 2\sin(\Delta\theta_{2z}^k) &= -\mathbf{y}_2^k\mathbf{X} + \mathbf{x}_2^k\mathbf{Y} \end{aligned} \tag{78}$$

3.3. The vector of relative displacements ($\mathbf{u}_r^i$) is assembled on the local system of the element from the nodal relative displacements ($\Delta\mathbf{u}_{e1}^k$ and $\Delta\mathbf{u}_{e2}^k$) and rotation vectors ($\Delta\boldsymbol{\theta}_1^k$ and $\Delta\boldsymbol{\theta}_2^k$) of each layer. For a given layer-k, vector $\mathbf{u}_r^k$ is obtained as:

$$\begin{aligned} u_{r(j)}^k &= \Delta u_{e1(j)}^k, & j &= 1 \text{ to } 3 \\ u_{r(j+3)}^k &= \Delta\theta_{1(j)}^k, & j &= 1 \text{ to } 3 \\ u_{r(7)}^k &= \Delta u_{e2(1)}^k + \Delta\ell^i \\ u_{r(j+6)}^k &= \Delta u_{e2(j)}^k, & j &= 2 \text{ to } 3 \\ u_{r(j+9)}^k &= \Delta\theta_{2(j)}^k, & j &= 1 \text{ to } 3 \end{aligned} \tag{79}$$

3.4. The vector of relative displacements ($\mathbf{u}_p^i$), used in the calculation of penalty internal forces, is assembled. This vector refers to relative displacements in two different reference systems, one for each node, and is assembled from the nodal displacements vectors of each layer ($\Delta\mathbf{u}_{n1}^k$ and $\Delta\mathbf{u}_{n2}^k$). The vector $\mathbf{u}_p^k$, for layer-k, is obtained as follows:

$$\begin{aligned} u_{p(j)}^k &= \Delta u_{n1(j)}^k, & j &= 1 \text{ to } 3 \\ u_{p(j+6)}^k &= \Delta u_{n2(1)}^k, & j &= 1 \text{ to } 3 \end{aligned} \tag{80}$$

4. Each part of the internal force vector is calculated in its corresponding reference systems and then transferred to global coordinate system as follows:

$$\begin{aligned} \mathbf{f}_{lay}^i &= \mathbf{K}_{lay}\mathbf{u}_r^i \\ \mathbf{f}_{int}^i &= \mathbf{K}_{int}\mathbf{u}_r^i \\ \mathbf{f}_p^i &= \mathbf{K}_p\mathbf{u}_p^i \end{aligned} \tag{81}$$

4.1. Total internal force vector, in the global reference system, is thus obtained

$$\mathbf{f}_g^i = \overline{\mathbf{R}}_\mathbf{e}^{(\mathbf{i})}(\mathbf{f}_\mathbf{lay}^\mathbf{i} + \mathbf{f}_\mathbf{int}^\mathbf{i}) + \overline{\mathbf{R}}_\mathbf{n}^{(\mathbf{i})}\mathbf{f}_\mathbf{p}^\mathbf{i} \tag{82}$$

where $\mathbf{f}_{lay}^i$ is the element internal force vector due to deformation at layers; $\mathbf{f}_{int}^i$ is the element internal force vector due to deformation at interfaces; $\mathbf{f}_p^i$ is the element internal force vector due to penalty method; and $\overline{\mathbf{R}}_\mathbf{e}^{(\mathbf{i})}$ and $\overline{\mathbf{R}}_\mathbf{n}^{(\mathbf{i})}$ are transformation matrices:

$$\overline{\mathbf{R}}_e^i = \begin{bmatrix} \mathbf{R}_e^i & 0 & 0 & 0 & 0 \\ 0 & \mathbf{R}_e^i & 0 & 0 & 0 \\ 0 & 0 & \mathbf{R}_e^i & 0 & 0 \\ 0 & 0 & 0 & \ddots & 0 \\ 0 & 0 & 0 & 0 & \mathbf{R}_e^i \end{bmatrix} \text{ and } \overline{\mathbf{R}}_n^i = \begin{bmatrix} \mathbf{R}_{n1}^i & 0 & 0 & 0 & 0 \\ 0 & \mathbf{R}_{n1}^i & 0 & 0 & 0 \\ 0 & 0 & \ddots & 0 & 0 \\ 0 & 0 & 0 & \mathbf{R}_{n2}^i & 0 \\ 0 & 0 & 0 & 0 & \mathbf{R}_{n2}^i \end{bmatrix} \tag{83}$$

5. The element stiffness matrix ($\mathbf{K}_e^i$) and penalty matrix ($\mathbf{K}_p^i$) are then assembled in their respective local coordinate systems, from the matrices of each layer and interface, and then transferred to the global coordinate system ($\mathbf{K}_g^i$):

$$\mathbf{K}_g^i = \overline{\mathbf{R}}_\mathbf{e}^{(\mathbf{i})\mathbf{T}}\mathbf{K}_\mathbf{e}^\mathbf{i}\overline{\mathbf{R}}_\mathbf{e}^{(\mathbf{i})} + \overline{\mathbf{R}}_\mathbf{n}^{(\mathbf{i})\mathbf{T}}\mathbf{K}_\mathbf{p}^\mathbf{i}\overline{\mathbf{R}}_\mathbf{n}^{(\mathbf{i})} \tag{84}$$

4. Numerical tests

The multilayer pipe beam element has been numerically implemented, according to the formulation presented in the previous sections. A number of representative analyses were carried out, to verify the element's performance.

4.1. Two layer pipe beam subjected to axial loading

A two layer straight beam, restrained at one end at the inner layer and loaded by an axial force F, applied at the free end of the outer layer, was considered in this example. The beam was modeled by 15 uniform finite elements, using material and cross section geometrical properties listed in Fig. 12. Each layer Young's modulus was set such that the axial stiffness at both layers are equal, i.e., $E_{int}A_{int} = E_oA_o$, resulting in symmetric interlayer shear stress distribution along the length, with respect to beam mid-section. Two studies considering possible slip conditions between layers were approached: the linear slip and the slip with static friction. In the first, a linear elastic constitutive model was used for the interface material resulting in a typical linear elastic analysis. And, in

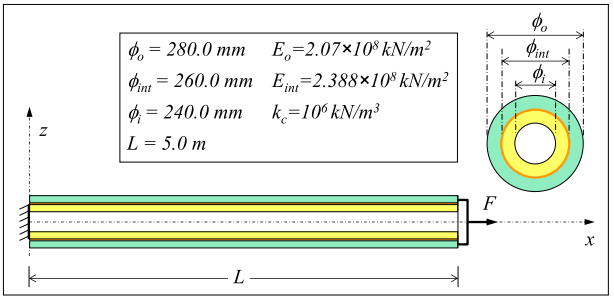

Fig. 12. The two layer pipe beam under axial loading.

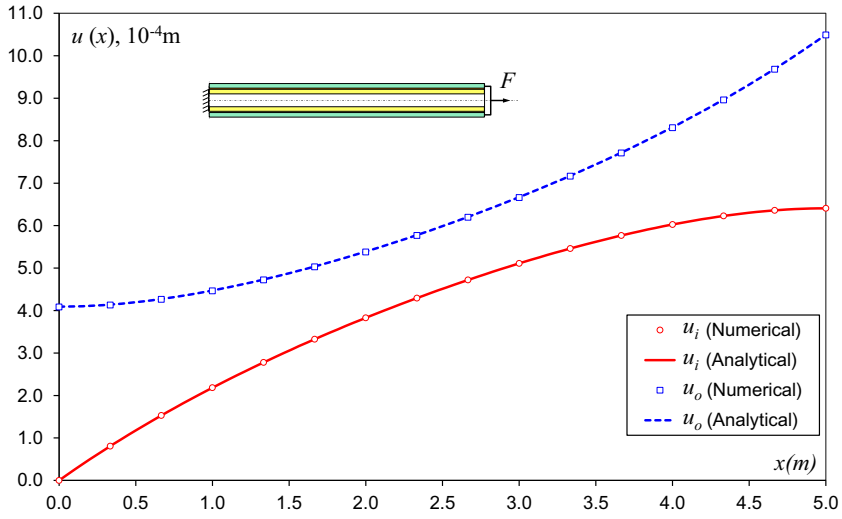

Fig. 13. Axial displacement distribution at each layer – linear elastic slip analysis.

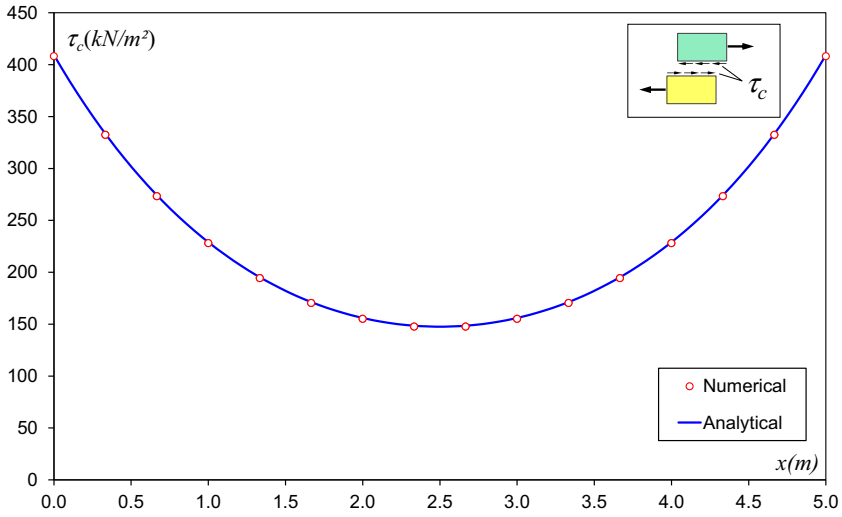

Fig. 14. Interlayer shear stress distribution – linear elastic slip analysis.

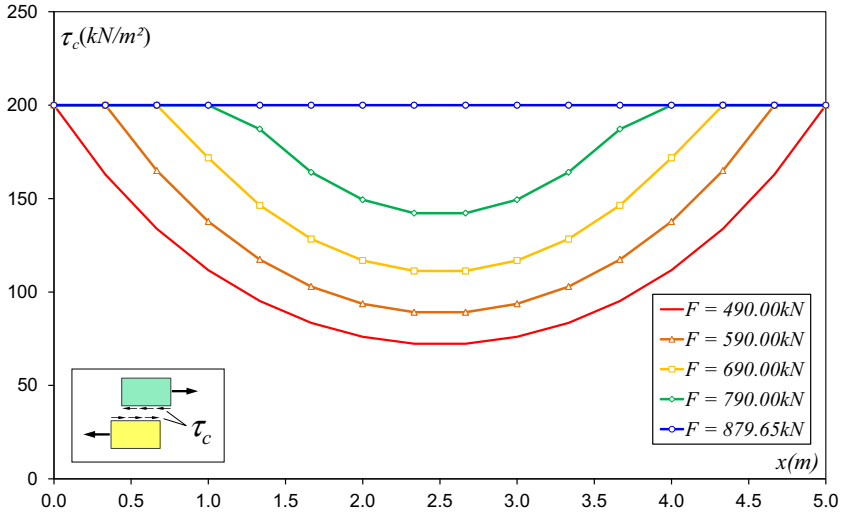

Fig. 15. Contact stresses at interface – slip with static friction.

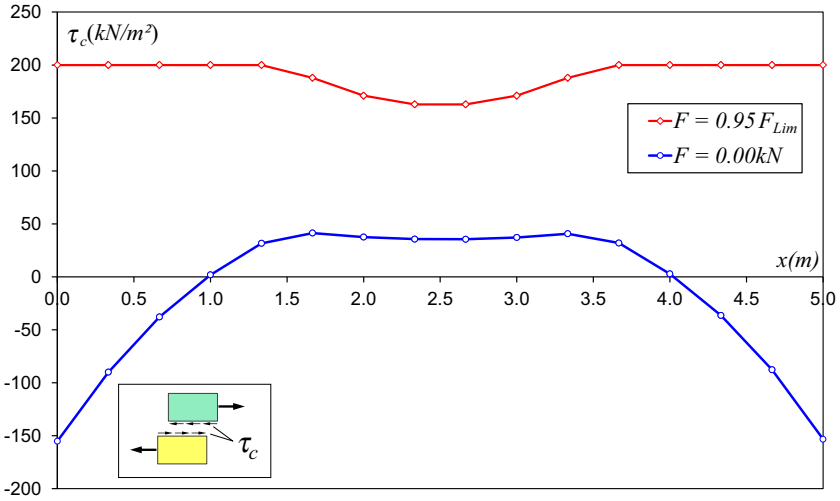

Fig. 16. Residual contact stresses at interface after unloading – slip with static friction.

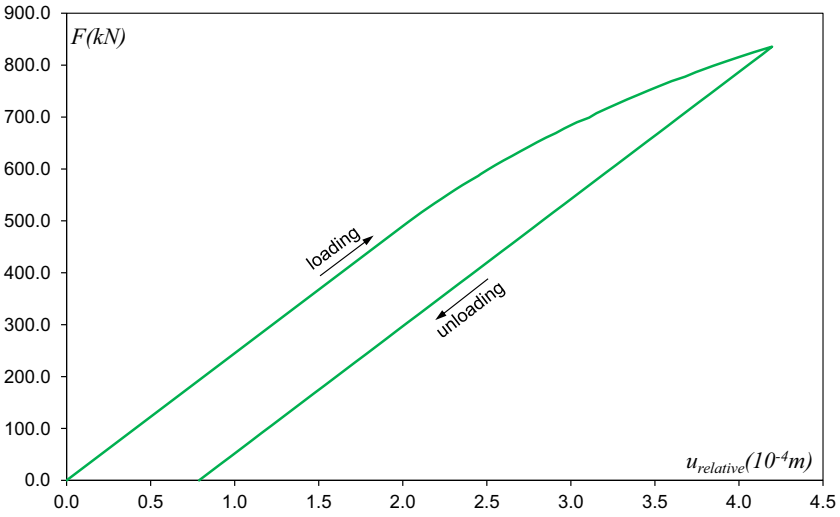

Fig. 17. Applied load vs. relative axial displacement at the beam tip – slip with static friction.

the second the elastic-perfect plastic material model was employed as in the derivations presented for case B, in Section 2.7.

In the linear elastic analysis an axial force $F = 1000$ kN was applied. Figs. 13 and 14 show obtained distribution results for the axial displacement at each layer of the beam and for the contact shear stress at the interface between layers, respectively. In these pictures the corresponding analytical solutions are also presented and a good agreement between the results is observed.

In the nonlinear analysis using the slip with static friction model, a limit contact shear stress $\tau_\ell = 200.0$ kN/m^2 was used. One of the analysis objectives is to evaluate the model solution results under axial loading, up to its theoretical limit $F_\ell = 2\pi r_{int} L \tau_\ell$. Starting from the elastic slip limit value $F = 490$ kN, the applied load history was set in 45 equal steps up to $F = 879.65$ kN. In Fig. 15 the contact stress distribution along the beam, for certain load values, is presented. From these results one can notice the adhesive material damage propagation, starting from both ends and towards the center of the beam, but still preserving symmetry. Fig. 16 shows the resulting residual contact stresses obtained after load $F = 0.95F_\ell$ has been applied and then removed. The nonlinear nature of the numerical response can also be observed in the load-end displacement plots in Fig. 17, for both layers.

4.2. Two-layer cantilever beam

In this example the behavior of a two layer cantilever pipe beam under pure bending loading, as shown in Fig. 18, is investigated. Considering an equivalent homogeneous beam, analytical solutions for the cross-section rotation (θ), horizontal (u) and vertical (w) displacements, at the tip of the beam, are given by [24]:

$$\theta = \frac{ML}{EI}, \quad u = L\left(\frac{\sin(\theta)}{\theta} - 1\right) \quad \text{and} \quad w = \frac{L}{\theta}(1 - \cos(\theta)) \tag{85}$$

In the analysis, interlayer contact conditions (linear elastic slip) are set with stiffness of $k_c = 10^6$ kN/m^3 and a bending moment M_y, required to curl the beam into a complete circle ($\theta = 2\pi$), is progres-

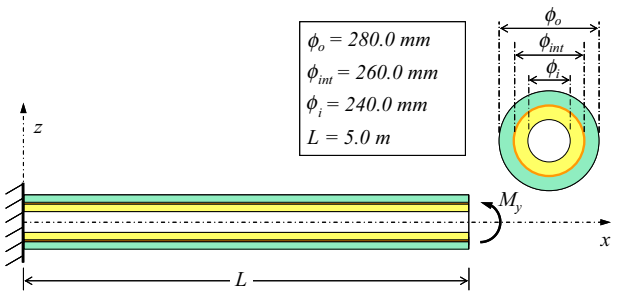

Fig. 18. The two-layer cantilever beam.

sively applied at the beam inner layer free end, in ten equal loading increments. The equivalent homogeneous beam bending stiffness is obtained from adding the inner and outer layer bending stiffness, i.e.: $(EI)_{eq} = E_i I_i + E_o I_o$. Considering the perfect binding condition between layers, stress analytical distributions along the pipe thickness may be obtained from:

$$\sigma_k = \frac{E_k M_y z}{(EI)_{eq}} \tag{86}$$

where k is layer index.

Fig. 19 presents bending moment distributions along the beam length, at each element layer, considering the same material for both layers, i.e.: $E_i = E_o = 200$ GPa. In these bending distributions required equilibrium conditions at each layer as well as the global beam equilibrium are satisfied.

Considering the mid-section of the beam, where pure bending moment occurs at each layer, the normal stress presents linear distribution along the pipe wall, as shown in the numerical results in Fig. 20. As indicated a good agreement with exact solutions for perfectly bonded beams, given by Eq. (86), is also observed.

If layers with different materials are considered (i.e.: $E_i = 2E_o = 200$ GPa), the bending moment distributions along the length of beam is as shown in Fig. 21. Considering the mid-section of the beam, normal stress distributions remain linear but discontinuous at the interface. As shown in Fig. 22 numerical and analytical solutions are in good agreement.

Fig. 23 shows obtained numerical displacement results as compared to the analytical solutions in Eqs. (85). A good agreement be-

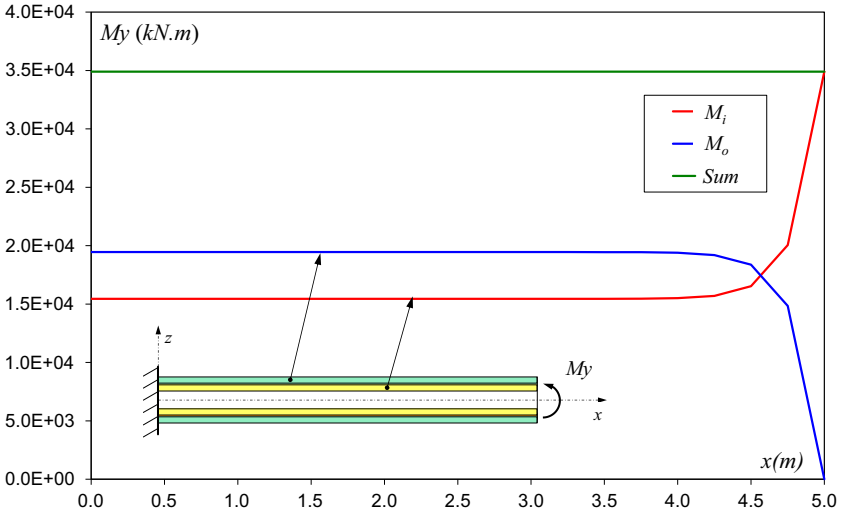

Fig. 19. Bending moment distributions (both layers with same material).

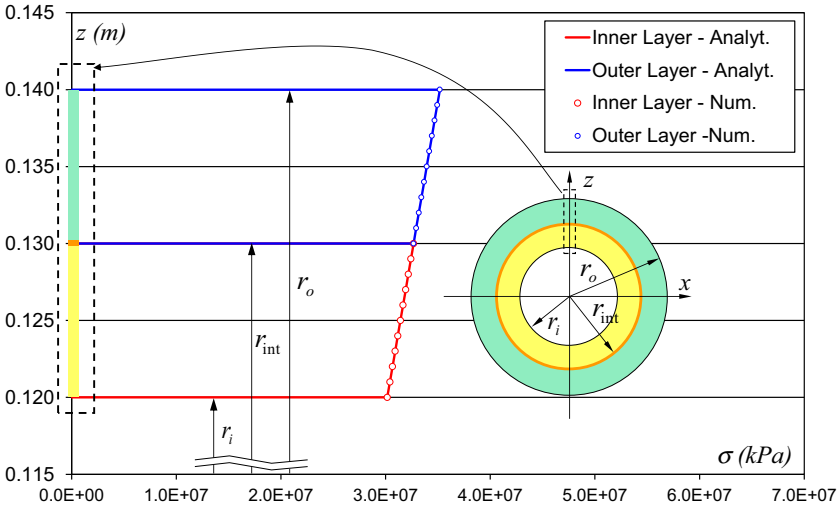

Fig. 20. Axial stress distributions at beam mid-section (both layers with same material).

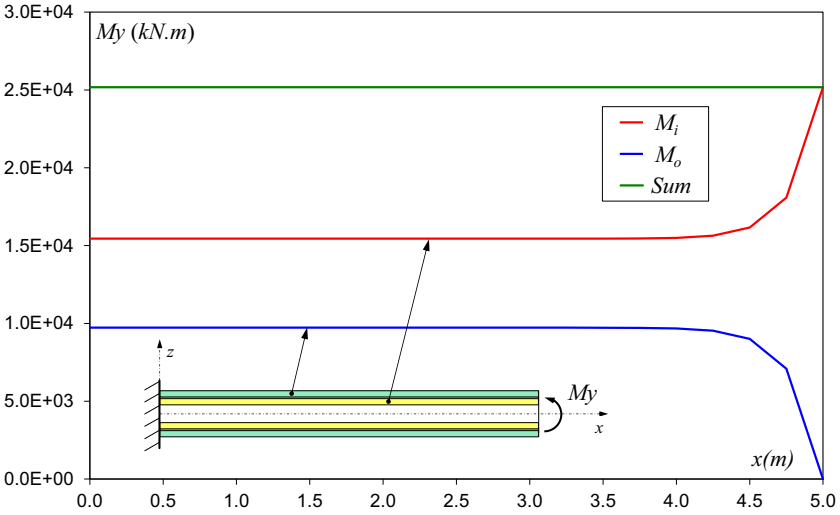

Fig. 21. Bending moment distributions (layers with different materials).

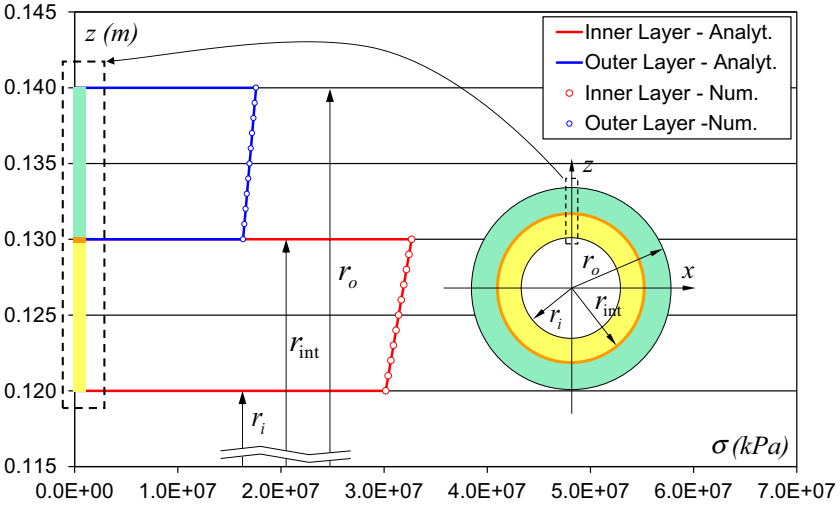

Fig. 22. Axial stress distribution at beam mid-section (layers with different materials).

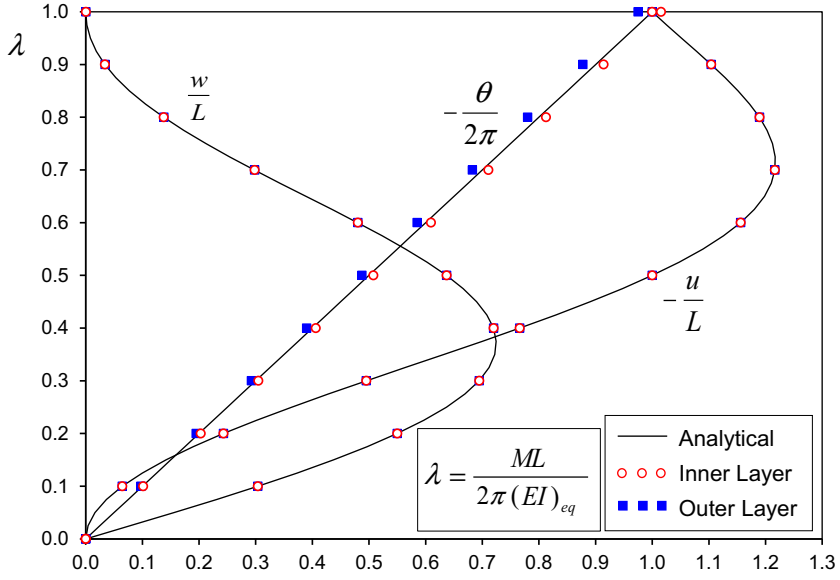

Fig. 23. Normalized displacements at the two-layer cantilever beam tip.

tween solutions is observed. It also indicates that the transverse displacement compatibility at both layers is well represented by the analysis results, as displacements at the tip of the beam are the same in both layers.

4.3. Flexible riser in catenary configuration

In this example a 350.0 m long flexible catenary riser is considered under in-plane analysis. The riser is connected at the top to a floating unit and at the bottom to a sub-sea tower which is located at a water depth of 150.0 m and horizontally displaced 150.0 m from the top connection. The riser is assumed to be fully filled of seawater. A finite element mesh with 20 elements was used, 16 equal elements with a length of 20.0 m, 2 elements with 10.0 m and 2 with 5.0 m. The geometrical and material properties used in this model, as well as the detailed finite element mesh considered, are shown in Fig. 24. The same riser system has already been analyzed in various publications [25–27].

In the present study the riser was modeled using three element layers, with properties shown in Table 2. A flexible riser is a composite construction of interlocked steel and polymeric layers designed to give the structure an axial stiffness approximately five orders of magnitude greater than its bending stiffness. Thus, to reproduce the stiffness properties presented in Fig. 24, a stiffening factor (EA/EI) was used for all layers.

A static analysis has been carried out considering self-weight and buoyancy forces only. Horizontal and vertical reaction forces at the supporting points are listed in Table 3 and the bending moment diagram along the length of the riser is shown in Fig. 25. Solution results for the present model are presented for each individual layer and for the total sum, which is in good agreement with

Table 3
Support reactions at top and bottom connections.

Reference	V_{bottom} (kN)	V_{top} (kN)	H_{bottom} (kN)	H_{top} (kN)
McNamara et al. (FEM)	35.83	91.45	11.92	11.57
McNamara et al. (cable)	35.77	91.51	12.02	12.02
Yazdchi and Crisfield	35.86	91.61	12.04	12.04
Present work				
Inner	12.60	30.34	3.85	3.83
Middle	1.36	3.45	0.45	0.45
Outer	21.88	57.84	7.72	7.74
Sum	**35.84**	**91.63**	**12.02**	**12.02**

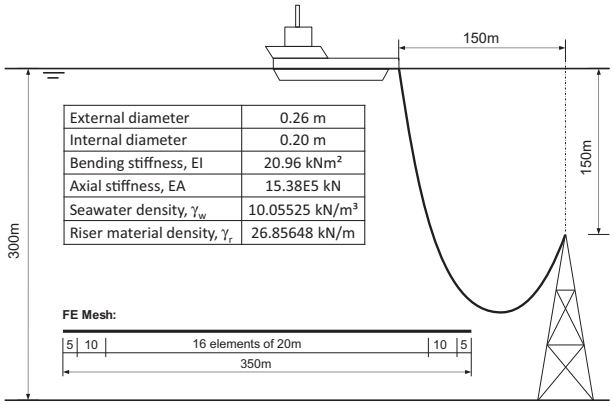

Fig. 24. Flexible riser in catenary configuration.

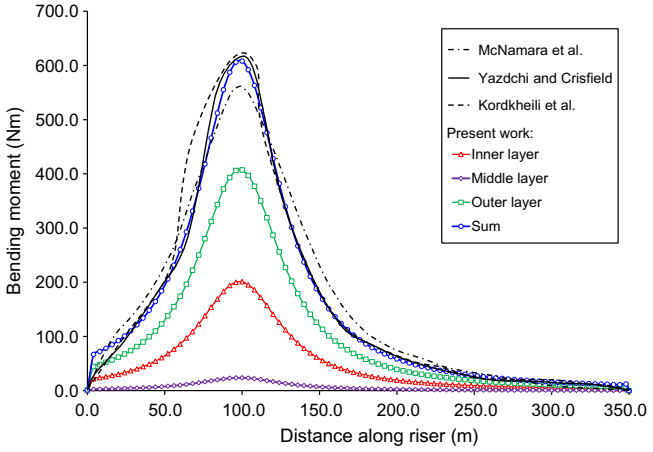

Fig. 25. Bending moment distribution along multilayered riser.

Table 2
Multilayer riser properties.

Internal diameter, D_i	0.20 m
External diameter, D_o	0.26 m
Inner layer thickness, t_i	0.003 m
Middle layer thickness, t_m	0.024 m
Outer layer thickness, t_o	0.003 m
Inner layer Young modulus, E_i	6.76E+05 kN/m^2
Middle layer Young modulus, E_m	6.76E+03 kN/m^2
Outer layer Young modulus, E_o	6.76E+05 kN/m^2
Inner layer density, γ_i	129.12 kN/m^3
Middle layer density, γ_m	1.2912 kN/m^3
Outer layer density, γ_o	129.12 kN/m^3
Stiffening factor, (EA/EI)	7.3378E+04
Contact stiffness, k_c	1.0E+06 kN/m^3

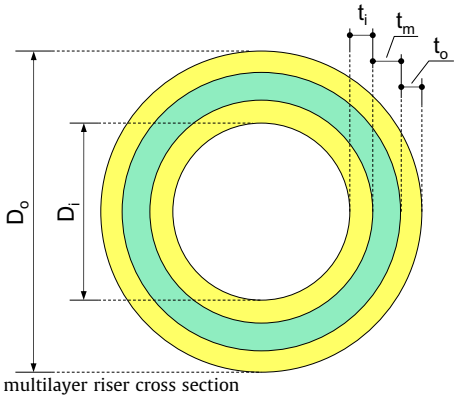

the solutions given by McNamara et al. [25] and Yazdchi and Crisfield [26], what verifies the accuracy of the element model.

5. Concluding remarks

In this paper, a multilayered beam element for large displacement analysis of risers and pipelines has been presented. Its main features include the possibility of modeling a multilayered pipe cross section in detail and representing the slip condition between layers, including friction. The element allows representation of both bonded and unbonded pipes. For the unbonded model, the number of degrees-of-freedom is proportional to the number of element layers. The global results are in agreement with traditional beam formulations available in the literature. Additionally, the element provides detailed information on local results such as stress distribution and internal forces at each pipe layer, and also the contact stress distribution between layers. The new pipe beam formulation provides the detailed representation of multilayered pipes, yet remains efficient, even with the additional degrees-of-freedom of each layer, in large displacement analysis of pipelines.

Appendix A. Nomenclature

i	vector index; node index; iteration
t	time
X, Y, Z	local element reference system
x, y, z	nodal reference system; local coordinates on element cross section
k	element layer index
N_{layers}	number of layers
$\boldsymbol{\theta}$	pseudo-vector of rotation
θ_x, θ_y, θ_z	components of rotations about X, Y and Z axis, respectively
u	displacement vector
u, v, w	components of displacements in the X, Y and Z directions, respectively
ϕ_i	Hermitian polynomials
ξ	element coordinate in the longitudinal (X) direction
ℓ	element length
β	generalized degree-of-freedom for shear strain
H	interpolation matrix
ε_{xx}	normal strain component
γ_{xy}, γ_{xz}	shear strain components
e_{ij}	(i,j) linear strain components
η_{ij}	(i,j) nonlinear strain components
$\mathbf{B}_L$	compatibility matrix for linear strains
$\mathbf{K}_L$	linear stiffness matrix
$\mathbf{C}$	linear-elastic constitutive tensor
φ	angular coordinate at layer or interface cross section
E^k	layer material Young modulus
G^k	layer material shear modulus
A^k	layer cross section area
I^k	layer cross section moment of inertia with respect to the axis of symmetry
J^k	layer cross section polar moment of inertia with respect to the geometric center
$\mathbf{K}_G$	geometric (nonlinear) stiffness matrix
$\mathbf{B}_G$	geometric compatibility matrix
τ	stress components matrix
τ_{xx}	normal stress component
τ_{xy}, τ_{xz}	shear stresses components
$\overline{\boldsymbol{\gamma}}_i$	interlayer slip vector
$\overline{\gamma}_x$	longitudinal slip component
$\overline{\gamma}_\varphi$	circumferential slip component
k_c	contact stiffness between layers (slip modulus)
k_c^{ep}	nonlinear slip modulus
τ_x, τ_φ	contact stresses between layers in longitudinal an circumferential directions, respectively
$\mathbf{K}_i$	interface stiffness matrix
k^p	penalty parameter
$\mathbf{K}_p$	penalty stiffness matrix
$\mathbf{K}_e$	element stiffness matrix in the local system
$\mathbf{K}_g$	element stiffness matrix in the global system
$\mathbf{f}_e$	element internal forces vector in the local system
$\mathbf{f}_p$	penalty internal forces vector in the local system
$\mathbf{f}_g$	element internal forces vector in the global system
$\mathbf{K}$	stiffness matrix for the whole structure in the global system
$\mathbf{U}$	displacement vector for the whole structure in the global system
R	external forces vector in the global system
$\mathbf{F}$	internal forces vector for the whole structure in the global system
$\mathbf{R}_e$	element rotation matrix
$\mathbf{R}_n$	nodal rotation matrix

Appendix B. Element matrices

B.1. Element interpolation matrix

From Eq. (21), the element interpolation matrix results in:

$$\mathbf{H}^k(\xi,y,z)=\begin{bmatrix} 1-\frac{\xi}{\ell} & \frac{6y}{\ell}\phi_1 & \frac{6z}{\ell}\phi_1 & 0 & z\phi_2 & -y\phi_2 & \frac{\xi}{\ell} & -\frac{6y}{\ell}\phi_1 & -\frac{6z}{\ell}\phi_1 & 0 & -z\phi_3 & y\phi_3 & (1-6\phi_1)z & (1-6\phi_1)y \\ 0 & \phi_4 & 0 & -\left(1-\frac{\xi}{\ell}\right)z & 0 & \ell\phi_5 & 0 & \phi_6 & 0 & -\frac{\xi}{\ell}z & 0 & -\xi\phi_1 & 0 & (\xi-\ell\phi_7) \\ 0 & 0 & \phi_4 & \left(1-\frac{\xi}{\ell}\right)y & -\ell\phi_5 & 0 & 0 & 0 & \phi_6 & \frac{\xi}{\ell}y & \xi\phi_1 & 0 & (\xi-\ell\phi_7) & 0 \end{bmatrix}_{3\times 14} \tag{B.1}$$

B.2. Linear compatibility matrix

The linear compatibility matrix is obtained from Eqs. (25), (27), and (29), which results in:

$$\mathbf{B}_L^k = \begin{bmatrix} -\frac{1}{\ell} & \frac{6y}{\ell}\frac{d\phi_1}{d\xi} & \frac{6z}{\ell}\frac{d\phi_1}{d\xi} & 0 & z\frac{d\phi_2}{d\xi} & -y\frac{d\phi_2}{d\xi} & \frac{1}{\ell} & -\frac{6y}{\ell}\frac{d\phi_1}{d\xi} & -\frac{6z}{\ell}\frac{d\phi_1}{d\xi} & 0 & -z\frac{d\phi_3}{d\xi} & y\frac{d\phi_3}{d\xi} & -6z\frac{d\phi_1}{d\xi} & -6y\frac{d\phi_1}{d\xi} \\ 0 & 0 & 0 & \frac{z}{\ell} & 0 & \ell\frac{d\phi_5}{d\xi} - \phi_2 & 0 & 0 & 0 & -\frac{z}{\ell} & 0 & \phi_3 - \phi_1 - \xi\frac{d\phi_1}{d\xi} & 0 & 2 - 6\phi_1 - \ell\frac{d\phi_7}{d\xi} \\ 0 & 0 & 0 & -\frac{y}{\ell} & \phi_2 - \ell\frac{d\phi_5}{d\xi} & 0 & 0 & 0 & 0 & \frac{y}{\ell} & \phi_1 - \phi_3 + \xi\frac{d\phi_1}{d\xi} & 0 & 2 - 6\phi_1 - \ell\frac{d\phi_7}{d\xi} & 0 \end{bmatrix}_{3\times 14} \tag{B.2}$$

B.3. Nonlinear compatibility matrix

The nonlinear (geometric) compatibility matrix is defined as:

$$\mathbf{B}_G^k = \begin{bmatrix} -\frac{1}{\ell} & \frac{6y}{\ell}\frac{d\phi_1}{d\xi} & \frac{6z}{\ell}\frac{d\phi_1}{d\xi} & 0 & z\frac{d\phi_2}{d\xi} & -y\frac{d\phi_2}{d\xi} & \frac{1}{\ell} & -\frac{6y}{\ell}\frac{d\phi_1}{d\xi} & -\frac{6z}{\ell}\frac{d\phi_1}{d\xi} & 0 & -z\frac{d\phi_3}{d\xi} & y\frac{d\phi_3}{d\xi} & -6z\frac{d\phi_1}{d\xi} & -6y\frac{d\phi_1}{d\xi} \\ 0 & \frac{d\phi_4}{d\xi} & 0 & \frac{z}{\ell} & 0 & \ell\frac{d\phi_5}{d\xi} & 0 & \frac{d\phi_6}{d\xi} & 0 & -\frac{z}{\ell} & 0 & -\phi_1 - \xi\frac{d\phi_1}{d\xi} & 0 & 1 - \ell\frac{d\phi_7}{d\xi} \\ 0 & 0 & \frac{d\phi_4}{d\xi} & -\frac{y}{\ell} & -\ell\frac{d\phi_5}{d\xi} & 0 & 0 & 0 & \frac{d\phi_6}{d\xi} & \frac{y}{\ell} & \phi_1 + \xi\frac{d\phi_1}{d\xi} & 0 & 1 - \ell\frac{d\phi_7}{d\xi} & 0 \\ 0 & \frac{6}{\ell}\phi_1 & 0 & 0 & 0 & -\phi_2 & 0 & -\frac{6}{\ell}\phi_1 & 0 & 0 & 0 & \phi_3 & 0 & 1 - 6\phi_1 \\ 0 & 0 & 0 & 1 - \frac{\xi}{\ell} & 0 & 0 & 0 & 0 & 0 & \frac{\xi}{\ell} & 0 & 0 & 0 & 0 \\ 0 & 0 & \frac{6}{\ell}\phi_1 & 0 & \phi_2 & 0 & 0 & 0 & -\frac{6}{\ell}\phi_1 & 0 & -\phi_3 & 0 & 1 - 6\phi_1 & 0 \\ 0 & 0 & 0 & \frac{\xi}{\ell} - 1 & 0 & 0 & 0 & 0 & 0 & -\frac{\xi}{\ell} & 0 & 0 & 0 & 0 \end{bmatrix}_{7\times 14} \tag{B.3}$$

with $y = r\cos\varphi$ and $z = r\sin\varphi$.

B.4. Interface compatibility matrix

The interface compatibility matrix is defined as:

$$\mathbf{B}_i^k = \begin{bmatrix} \frac{\xi}{\ell} - 1 & 0 & -z\phi_2 & y\phi_2 & -\frac{\xi}{\ell} & 0 & z\phi_3 & -y\phi_3 & 1 - \frac{\xi}{\ell} & 0 & z\phi_2 & -y\phi_2 & \frac{\xi}{\ell} & 0 & -z\phi_3 & y\phi_3 & (6\phi_1 - 1)z & (6\phi_1 - 1)y & (1 - 6\phi_1)z & (1 - 6\phi_1)y \\ 0 & r\left(\frac{\xi}{\ell} - 1\right) & 0 & 0 & 0 & -r\frac{\xi}{\ell} & 0 & 0 & 0 & r\left(1 - \frac{\xi}{\ell}\right) & 0 & 0 & 0 & r\frac{\xi}{\ell} & 0 & 0 & 0 & 0 & 0 & 0 \end{bmatrix}_{2\times 20} \tag{B.4}$$

B.5. Linear stiffness matrix

By solving the integrals in Eq. (34), one rewrites linear stiffness matrix for element layer-k, as follows:

$$\mathbf{K}_L^k = \begin{bmatrix}
\frac{E^kA^k}{\ell} & 0 & 0 & 0 & 0 & 0 & -\frac{E^kA^k}{\ell} & 0 & 0 & 0 & 0 & 0 & 0 & 0 \\
 & \frac{12E^kI^k}{\ell^3} & 0 & 0 & 0 & \frac{6E^kI^k}{\ell^2} & 0 & -\frac{12E^kI^k}{\ell^3} & 0 & 0 & 0 & \frac{6E^kI^k}{\ell^2} & 0 & -\frac{12E^kI^k}{\ell^2} \\
 & & \frac{12E^kI^k}{\ell^3} & 0 & -\frac{6E^kI^k}{\ell^2} & 0 & 0 & 0 & -\frac{12E^kI^k}{\ell^3} & 0 & -\frac{6E^kI^k}{\ell^2} & 0 & -\frac{12E^kI^k}{\ell^2} & 0 \\
 & & & \frac{G^kJ^k}{\ell} & 0 & 0 & 0 & 0 & 0 & -\frac{G^kJ^k}{\ell} & 0 & 0 & 0 & 0 \\
 & & & & \frac{4E^kI^k}{\ell} & 0 & 0 & 0 & \frac{6E^kI^k}{\ell^2} & 0 & \frac{2E^kI^k}{\ell} & 0 & \frac{6E^kI^k}{\ell} & 0 \\
 & & & & & \frac{4E^kI^k}{\ell} & 0 & -\frac{6E^kI^k}{\ell^2} & 0 & 0 & 0 & \frac{2E^kI^k}{\ell} & 0 & -\frac{6E^kI^k}{\ell} \\
 & & & & & & \frac{E^kA^k}{\ell} & 0 & 0 & 0 & 0 & 0 & 0 & 0 \\
 & & & & & & & \frac{12E^kI^k}{\ell^3} & 0 & 0 & 0 & -\frac{6E^kI^k}{\ell^2} & 0 & \frac{12E^kI^k}{\ell^2} \\
 & & & & & & & & \frac{12E^kI^k}{\ell^3} & 0 & \frac{6E^kI^k}{\ell^2} & 0 & \frac{12E^kI^k}{\ell^2} & 0 \\
 & & & & & & & & & \frac{G^kJ^k}{\ell} & 0 & 0 & 0 & 0 \\
 & & & & & & & & & & \frac{4E^kI^k}{\ell} & 0 & \frac{6E^kI^k}{\ell} & 0 \\
 & & & & & & & & & & & \frac{4E^kI^k}{\ell} & 0 & -\frac{6E^kI^k}{\ell} \\
 & & & & & & & & & & & & \frac{12E^kI^k}{\ell} + G^kA^k\ell & 0 \\
 & & & & & & & & & & & & & \frac{12E^kI^k}{\ell} + G^kA^k\ell
\end{bmatrix} \quad \text{(B.5)}$$

where E^k and G^k are material Young and shear modulus of layer-k, respectively; A^k, I^k and J^k are cross section area, moment of inertia with respect to the cross-section axis of symmetry, and polar moment of inertia with respect to the layer-k geometric center, respectively.

B.6. Geometric stiffness matrix

Accordingly, the stiffness matrix associated to the nonlinear strain components defined in Eq. (11) is obtained as:

$$\mathbf{K}_G^k = \begin{bmatrix}
-\frac{F_1^k}{\ell} & 0 & 0 & 0 & -\frac{F_5^k}{\ell} & -\frac{F_6^k}{\ell} & \frac{F_1^k}{\ell} & 0 & 0 & 0 & \frac{F_5^k}{\ell} + F_3^k & \frac{F_6^k}{\ell} - F_2^k & F_3^k & F_2^k \\
 & -C_1F_1^k & 0 & \frac{F_5^k}{\ell} & -\frac{F_4^k}{\ell} & -C_2F_1^k & 0 & C_1F_1^k & 0 & -\frac{F_5^k}{\ell} - F_3^k & \frac{F_4^k}{\ell} & -C_2F_1^k & 0 & C_1\ell F_1^k \\
 & & -C_1F_1^k & \frac{F_6^k}{\ell} & C_2F_1^k & -\frac{F_4^k}{\ell} & 0 & 0 & C_1F_1^k & F_2^k - \frac{F_6^k}{\ell} & C_2F_1^k & \frac{F_4^k}{\ell} & C_1\ell F_1^k & 0 \\
 & & & -\frac{JF_1^k}{A\ell} & \frac{\ell F_5^k}{6} & \frac{\ell F_3^k}{6} & 0 & -\frac{F_5^k}{\ell} & -\frac{F_6^k}{\ell} & \frac{JF_1^k}{A\ell} & -\frac{\ell F_5^k}{6} & -\frac{\ell F_3^k}{6} & -F_6^k & -F_5^k \\
 & & & & -C_3F_1^k & 0 & \frac{F_5^k}{\ell} & \frac{F_4^k}{\ell} & -C_2F_1^k & -\frac{\ell F_2^k}{6} & C_4F_1^k & -\frac{F_4^k}{2} & -C_2\ell F_1^k & \frac{F_4^k}{2} \\
 & & & & & -C_3F_1^k & \frac{F_6^k}{\ell} & C_2F_1^k & \frac{F_4^k}{\ell} & -\frac{\ell F_3^k}{6} & \frac{F_4^k}{2} & C_4F_1^k & \frac{F_4^k}{2} & C_2\ell F_1^k \\
 & & & & & & -\frac{F_1^k}{\ell} & 0 & 0 & 0 & -F_3^k - \frac{F_5^k}{\ell} & F_2^k - \frac{F_6^k}{\ell} & -F_3^k & -F_2^k \\
 & & & & & & & -C_1F_1^k & 0 & F_3^k + \frac{F_5^k}{\ell} & -\frac{F_4^k}{\ell} & C_2F_1^k & 0 & -C_1\ell F_1^k \\
 & & & & & & & & -C_1F_1^k & \frac{F_6^k}{\ell} - F_2^k & -C_2F_1^k & -\frac{F_4^k}{\ell} & -C_1\ell F_1^k & 0 \\
 & & & & & & & & & -\frac{JF_1^k}{A\ell} & \frac{\ell F_5^k}{6} & \frac{\ell F_3^k}{6} & F_6^k - \ell F_2^k & F_5^k + \ell F_3^k \\
 & & & & & & & & & & -C_3F_1^k & 0 & -C_2\ell F_1^k & -\frac{F_4^k}{2} \\
 & & & & & & & & & & & -C_3F_1^k & -\frac{F_4^k}{2} & C_2\ell F_1^k \\
 & & & & & & & & & & & & -C_1\ell^2F_1^k & 0 \\
 & & & & & & & & & & & & & -C_1\ell^2F_1^k
\end{bmatrix} \quad \text{(B.6)}$$

with:

$$C_1 = \left(\frac{6}{5\ell} + \frac{12I^k}{A^k\ell^3}\right), \quad C_2 = \left(\frac{1}{10} + \frac{6I^k}{A^k\ell^2}\right),$$
$$C_3 = \left(\frac{2\ell}{15} + \frac{4I^k}{A^k\ell}\right) \quad \text{and} \quad C_4 = \left(\frac{\ell}{30} - \frac{2I^k}{A^k\ell}\right)$$

B.7. Interface stiffness matrix

The stiffness matrix for interface-*k*, considering a linear-elastic slip model is given by:

$$\mathbf{K}_i^k = \pi k_c^k \ell \begin{bmatrix}
\frac{2r}{3} & 0 & 0 & 0 & \frac{r}{3} & 0 & 0 & 0 & -\frac{2r}{3} & 0 & 0 & 0 & -\frac{r}{3} & 0 & 0 & 0 & 0 & 0 & 0 & 0 \\
 & \frac{2r^3}{3} & 0 & 0 & 0 & \frac{r^3}{3} & 0 & 0 & 0 & -\frac{2r^3}{3} & 0 & 0 & 0 & -\frac{r^3}{3} & 0 & 0 & 0 & 0 & 0 & 0 \\
 & & \frac{2r^3}{15} & 0 & 0 & 0 & -\frac{r^3}{30} & 0 & 0 & 0 & -\frac{2r^3}{15} & 0 & 0 & 0 & \frac{r^3}{30} & 0 & \frac{r^3}{10} & 0 & -\frac{r^3}{10} & 0 \\
 & & & \frac{2r^3}{15} & 0 & 0 & 0 & -\frac{r^3}{30} & 0 & 0 & 0 & -\frac{2r^3}{15} & 0 & 0 & 0 & \frac{r^3}{30} & 0 & -\frac{r^3}{10} & 0 & \frac{r^3}{10} \\
 & & & & \frac{2r}{3} & 0 & 0 & 0 & -\frac{r}{3} & 0 & 0 & 0 & -\frac{2r}{3} & 0 & 0 & 0 & 0 & 0 & 0 & 0 \\
 & & & & & \frac{2r^3}{3} & 0 & 0 & 0 & -\frac{r^3}{3} & 0 & 0 & 0 & -\frac{2r^3}{3} & 0 & 0 & 0 & 0 & 0 & 0 \\
 & & & & & & \frac{2r^3}{15} & 0 & 0 & 0 & \frac{r^3}{30} & 0 & 0 & 0 & -\frac{2r^3}{15} & 0 & \frac{r^3}{10} & 0 & -\frac{r^3}{10} & 0 \\
 & & & & & & & \frac{2r^3}{15} & 0 & 0 & 0 & \frac{r^3}{30} & 0 & 0 & 0 & -\frac{2r^3}{15} & 0 & -\frac{r^3}{10} & 0 & \frac{r^3}{10} \\
 & & & & & & & & \frac{2r}{3} & 0 & 0 & 0 & \frac{r}{3} & 0 & 0 & 0 & 0 & 0 & 0 & 0 \\
 & & & & & & & & & \frac{2r^3}{3} & 0 & 0 & 0 & \frac{r^3}{3} & 0 & 0 & 0 & 0 & 0 & 0 \\
 & & & & & & & & & & \frac{2r^3}{15} & 0 & 0 & 0 & -\frac{r^3}{30} & 0 & -\frac{r^3}{10} & 0 & \frac{r^3}{10} & 0 \\
 & & & & & & & & & & & \frac{2r^3}{15} & 0 & 0 & 0 & -\frac{r^3}{30} & 0 & \frac{r^3}{10} & 0 & -\frac{r^3}{10} \\
 & & & & & & & & & & & & \frac{2r}{3} & 0 & 0 & 0 & 0 & 0 & 0 & 0 \\
 & & & & & & & & & & & & & \frac{2r^3}{3} & 0 & 0 & 0 & 0 & 0 & 0 \\
 & & & & & & & & & & & & & & \frac{2r^3}{15} & 0 & -\frac{r^3}{10} & 0 & \frac{r^3}{10} & 0 \\
 & & & & & & & & & & & & & & & \frac{2r^3}{15} & 0 & \frac{r^3}{10} & 0 & -\frac{r^3}{10} \\
 & & & & & & & & & & & & & & & & \frac{r^3}{5} & 0 & -\frac{r^3}{5} & 0 \\
 & & & & & & & & & & & & & & & & & \frac{r^3}{5} & 0 & -\frac{r^3}{5} \\
 & & & & & & & & & & & & & & & & & & \frac{r^3}{5} & 0 \\
 & & & & & & & & & & & & & & & & & & & \frac{r^3}{5}
\end{bmatrix} \tag{B.7}$$

symmetric

References

[1] Newmark NM, Siess CP, Viest IM. Tests and analysis of composite beams with incomplete interactions. Proc Soc Exp Stress Anal 1951;9(1):75–92.
[2] Schnabl S, Saje M, Turk G, Planinc I. Analytical solution of two-layer beam taking into account interlayer slip and shear deformation. J Struct Eng 2007;133(6):886–94.
[3] Foraboschi P. Analytical solution of two-layer beam taking into account nonlinear interlayer slip. J Eng Mech 2009;135(10):1129–46.
[4] Ecsedi I, Baksa A. Static analysis of composite beams with weak shear connection. Appl Math Modell 2011;35(4):1739–50.
[5] Girhammar UA, Gopu VKA. Composite beam-columns with interlayer slip – exact analysis. J Struct Eng 1993;119(4):1265–82.
[6] Girhammar UA, Pan D. Exact static analysis of partially composite beams and beam-columns. Int. J. Mech Sci 2007;49(2):239–55.
[7] Chen WQ, Wu Y-F, Xu RQ. State space formulation for composite beam-columns with partial interaction. Compos Sci Technol 2007;67(11–12):2500–12.
[8] Schnabl S, Saje M, Turk G, Planinc I. Locking-free two-layer Timoshenko beam element with interlayer slip. Finite Elem Anal Des 2007;43(9):705–14.
[9] Čas B, Saje M, Planinc I. Non-linear finite element analysis of composite planar frames with an interlayer slip. Comput Struct 2004;82(23–26):1901–12.
[10] Čas B, Saje M, Planinc I. Buckling of layered wood columns. Adv Eng Software 2007;38(8–9):586–97.
[11] Krawczyk P, Frey F. Large deflections of laminated beams with interlayer slips – part 1: model development. Int J Comput-Aided Eng Software 2007;24(1):17–32.
[12] Krawczyk P, Frey F. Large deflections of laminated beams with interlayer slips – part 2: finite element development. Int J Comput-Aided Eng Software 2007;24(1):33–51.
[13] Zona A, Ranzi G. Finite element models for nonlinear analysis of steel–concrete composite beams with partial interaction in combined bending and shear. Finite Elem Anal Des 2011;47(2):98–118.
[14] Sousa Jr JBM, Silva AR. Analytical and numerical analysis of multilayered beams with interlayer slip. Eng Struct 2010;32(6):1671–80.
[15] Bathe KJ, Bolourchi S. Large displacement analysis of three-dimensional beam structures. Int J Numer Methods Eng 1979;14(7):961–86.
[16] Mourelle MM. Análise Dinâmica de Sistemas Estruturais Constituídos por Linhas Marítmas. COPPE/UFRJ, DSc, Engenharia Civil, 1993.
[17] Crisfield M. A consistent co-rotational formulation for non-linear, three-dimensional, beam-elements. Comput Methods Appl Mech Eng 1990;81(2):131–50.
[18] Pacoste C, Eriksson A. Beam elements in instability problems. Comput Methods Appl Mech Eng 1997;144(1–2):163–97.
[19] Bathe KJ. Finite element procedures. New Jersey: Prentice-Hall; 1996.

[20] Malvern LE. Introduction to the mechanics of a continuous medium. Prentice Hall; 1969.
[21] Simo JC, Hughes TJR. Computational inelasticity. New York: Springer-Verlag; 1998.
[22] Lages EN, Paulino GH, Menezes IFM, Silva RR. Nonlinear finite element analysis using an object-oriented philosophy – application to beam elements and to the cosserat continuum. Eng Comput 1999;15(1):73–89.
[23] Leon SE, Paulino GH, Pereira A, Menezes IFM, Lages EN. A unified library of nonlinear solution schemes. Appl Mech Rev 2011;64(4). Article 040803.
[24] Almeida CA, Albino JCR, Menezes IFM, Paulino GH. Geometric nonlinear analysis of functionally graded beams using a tailored lagrangian formulation. Mech Res Commun 2011;38(8):553–9.
[25] McNamara JF, O'Brien PJ, Gilroy SG. Non-linear analysis of flexible risers using hybrid finite elements. J Offshore Mech Arct Eng 1988;110(3):197–204.
[26] Yazdchi M, Crisfield MA. Non-linear dynamic behavior of flexible marine pipes and risers. Int. J. Numer. Methods Eng. 2002;54(9):1265–308.
[27] Kordkheili SAH, Bahai H, Mirtaheri M. An updated Lagrangian finite element formulation for large displacement dynamic analysis of three-dimensional flexible riser structures. Ocean Eng 2011;38(5–6):793–803.